Three-Dimensional Brownian Dynamics Simulator for the Study of Ion Permeation through Membrane Pores

Claudio Berti,*[†,‡] Simone Furini,[§] Dirk Gillespie,[†] Dezső Boda,[∥] Robert S. Eisenberg,[†] Enrico Sangiorgi,[‡] and Claudio Fiegna[‡]
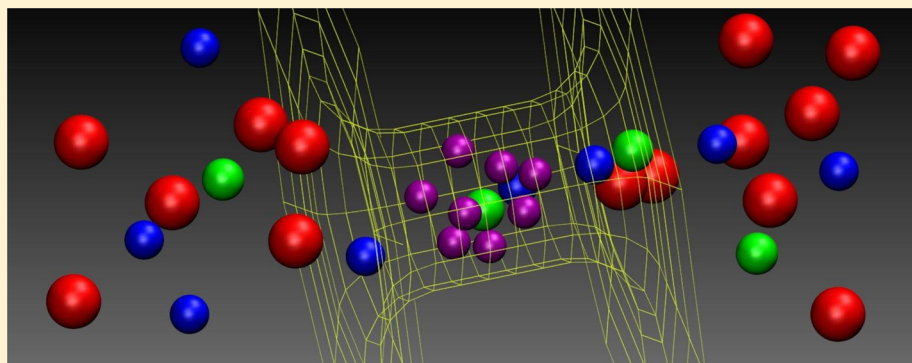
[†]Department of Molecular Biophysics and Physiology, Rush University Medical Center, Chicago,Illinois, United States
[‡]ARCES and DEI, University of Bologna and IUNET, Cesena, Italy
[§]Department of Medical Biotechnologies, University of Siena, Siena, Italy
[∥]Department of Physical Chemistry, University of Pannonia, Veszprém, Hungary

S *Supporting Information*

ABSTRACT: A three-dimensional numerical simulator based on Brownian dynamics (BD) for the study of ion transport through membrane pores is presented. Published BD implementations suffer from severe shortcomings in accuracy and efficiency. Such limitations arise largely from (i) the nonrigorous treatment of unphysical ion configurations; (ii) the assumption that ion motion occurs always in the high friction limit, (iii) the inefficient solution of the Poisson equation with dielectric interfaces, and (iv) the inaccurate treatment of boundary conditions for ion concentrations. Here, we introduce a new BD simulator in which these critical issues are addressed, implementing advanced techniques: (i) unphysical ion configurations are managed with a novel retracing technique; (ii) ion motion is evaluated integrating the Langevin equation with the algorithm of van Gunsteren and Berendsen (*Mol. Phys.* **1982**, *45*, 637−647); (iii) dielectric response in the Poisson equation is solved at run time with the Induced Charge Computation (ICC) method of Boda et al. (*J. Chem. Phys.* **2006**, *125*, 034901); and (iv) boundary conditions for ion concentrations are enforced by an accurate Grand Canonical Monte Carlo (GCMC) algorithm. Although some of these techniques have already been separately adopted for the simulation of membrane pores, our tool is the first BD implementation, to our knowledge, that fully retrace ions to avoid unphysical configurations and that computes dielectric interactions at each time step. Most other BD codes have been used on wide channels. Our BD simulator is specifically designed for narrow and crowded ion channels (e.g., L-type calcium channels) where all the aforementioned techniques are necessary for accurate results. In this paper, we introduce our tool, focusing on the implementation and testing of key features and we illustrate its capabilities through the analysis of test cases. The source code is available for download at www.phys.rush.edu/BROWNIES.

1. INTRODUCTION

Ion channels are integral membrane proteins that catalyze the diffusion of ions through the cell membrane. Any living organism, from bacteria to eukaryotes, contains a large number of ion channels, which are classified into families on the basis of the ionic species to which the channel is most permeable, (e.g., Na^+, K^+, and Ca^{2+}) and on the stimulus responsible for the opening/closing of the pore, (e.g., voltage-gated, ligand-gated, and mechanoreceptors).[1−4]

Ion channels are involved in a plethora of biological processes, from the transmission of electrical impulses in nerve cells to muscle contraction. In a very real sense, ion channels are the nanovalves of life, playing a role in biological function not so different from that of transistors in modern electronics.[5] Ion channel malfunctions are involved in several hereditary diseases, such as cystic fibrosis and long-QT syndrome or severe pathologies such as arrhythmia. As a result, ion channels are targets of numerous pharmaceutical compounds.[6−8]

The capability of ion channels to respond to different physicochemical stimuli has also inspired the design of hybrid sensors, in which ion channels are adopted as sensing units and electronic circuitry is used to detect the permeating currents.[9−12] Prototypes based on this setup have already been developed for the detection of molecules in solution[13−15] and, more recently, as an alternative to the current DNA-sequencing techniques.[16]

Solid-state nanopores are nanometer-scale pores set in electrically insulating membranes that can be used to study the transport properties of different ionic species or molecules in confined space.[17−19] Being much more stable and reliable than ion channels, they can be used to investigate some properties of ion permeation through biological membrane pores. Moreover, they can be used as detectors of specific molecules in electrolytic solutions. In this case, the detection principle is based on monitoring the variations of the ionic current flowing through the nanopore caused by the transit of a single molecule.[20−25] Nanopore sensors represent a very promising technology and a complete knowledge of ion permeation through such structures is needed.

Therefore, ion permeation through ion channels or synthetic pores, is a process of considerable importance and there is a need to determine its dependence of the structure of the pore. The numerical simulations of ion motion near and within membrane pores can enable the realistic estimation of their conductance and provide great insights on the particular aspects of ion permeation through such structures. For example, they can shed light on the concentration and velocity distribution of ions within the channel and can help to localize possible binding sites for ions inside the pore. Moreover, they allow one to study how different parameters affect ion permeation, and, therefore, to predict their influence on pore conductance and possibly identify critical ion channel mutations.

Different approaches can be employed to simulate ion permeation through membrane pores.[26−32] With all-atom models simulated by molecular dynamics (MD), it is possible to describe ion channels and electrolytic solutions at the atomistic level, explicitly modeling the interactions among all the simulated particles. Thus, MD should represent the most detailed approach to the simulation of ion transport through membrane pores,[33−38] but due to the huge computational burden, it allows the analysis of relatively small systems with large ionic concentrations and over extremely short time scales, too short in most cases for the estimation of transport properties such as channel conductance.[39−44]

The Poisson−Nernst−Planck model (PNP) is an approximation based on electrostatic continuity and the mean-field approximation. Ions are not explicitly treated as discrete particles but as continuous charge densities that represent the space-time average of the microscopic ion's charge. Ion flux inside the system is described by the Nernst−Planck (NP) equation. The self-consistency of this method is obtained by iteratively solving the Poisson equation and the NP equation.[27,40,45−57] This approach allows the calculation of conductance but deals approximately (at best) with many important aspects that influence ion translocation through narrow or crowded channels, such as ions' finite size and discrete charge.[40−42,48−50,58] The PNP model has been extended to include the effects of finite size ions in several different ways that give results comparable to Monte Carlo simulations for the same systems.[54,59−64] A newly developed

method in which the NP equation is coupled to Local Equilibrium Monte Carlo (LEMC) simulations (NP+LEMC) goes one step further.[62,65,66] It still uses the NP equation to describe transport, while the ionic distributions and the electrochemical potential profiles are computed on the basis of a molecular model, where ions are treated explicitly.

The Brownian dynamics (BD) approach represents an intermediate level of approximation between MD and PNP and offers a good trade-off between simulation accuracy and computation time for the analysis of ion currents flowing through nanometer-scale pores. BD also has the advantage over NP+LEMC that it simulates the dynamics of ions directly instead of just assuming an underlying transport equation.

BD is particularly well-suited for the use of the so-called primitive model of electrolytes. Within the primitive model, water is treated as a continuum; ions are spheres with finite size with their charges treated as discrete charges at spheres' centers.[67] Therefore, the BD approach explicitly models only the trajectories of all the ions inside the simulation domain, avoiding the computation of water molecules' trajectories.[29,68−73] The presence of water molecules is treated implicitly, considering only the average effect on the ions.

Furthermore, the pore, the membrane, and the charges inside the membrane are considered at fixed positions during the whole simulation. This allows BD to be much less computationally demanding than MD. On the other hand, with respect to PNP, BD takes into account ions' finite size and allows one to accurately model ion motion in narrow and crowded channels.

The BD approach allows the microsecond time scale simulation of membrane pores, and thus, it lends itself to the accurate and reliable estimation of their conductance.[40,42,43,51,70,74−85] For these reasons, BD simulations have been widely adopted to analyze conduction in membrane proteins or nanotubes, providing good agreement with experimental data.[43,49,75−77,82,86−88]

Although several implementations of BD have been proposed in the past,[42,43,77,80] improvements are still possible, in terms of both accuracy and efficiency. In particular, it is possible to identify critical aspects that, if underestimated, can easily lead to inaccurate or wrong results: (i) the handling of unphysical ion configurations; (ii) the integration of the Langevin equation of motion; (iii) the evaluation of the dielectric forces acting on the ions; and (iv) the treatment of boundary conditions for ion concentration in the solution baths.

Specifically, the treatment of unphysical ion configurations can introduce artifacts that can invalidate the simulation results. The inaccurate integration of the Langevin equation can produce a poor representation of the ions' Brownian motion and, as a consequence, meaningless simulation results since ions do not move according to the prescribed model. The imprecise computation of the electrostatic forces acting on the ions determines an inaccurate or wrong evaluation of ions' motion and therefore simulation results will be inaccurate or wrong as well. Finally, if boundary conditions for ion concentrations are not enforced correctly, the system is not simulated correctly. We focused on these issues in the attempt to improve the state of the art in this field.

The next sections describe how we tackled each of these critical points. Section 2.1 introduces our new technique to handle unphysical ion configurations. Section 2.2 illustrates the integration of the Langevin equation and the BD engine.
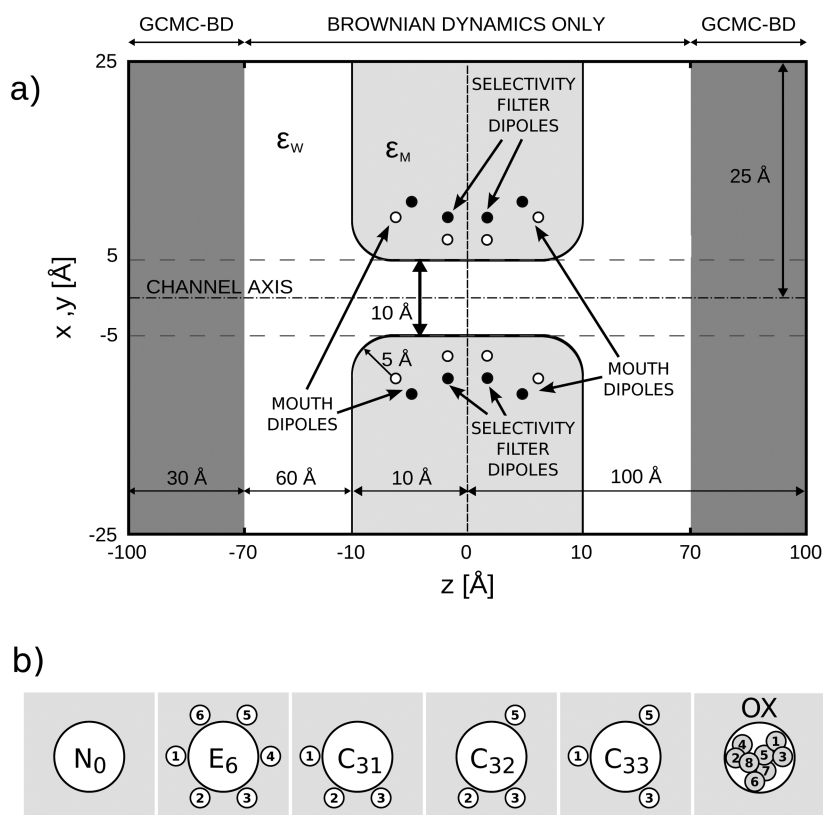
Figure 1. (a) 2-D simulation domain sketch. Water (white region) and membrane (light gray regions) feature different dielectric constants (ε_W = 80 and ε_M = 10, respectively). Two 30 Å width GCMC control cells (dark gray regions) are on either side of the membrane. White and black circles represent the negative and positive charges of dipole rings embedded in the membrane to mimic ion channel charged groups. We investigate ion permeation through this channel model for different configurations (N_0, E_6, C_{31}, C_{32}, and C_{33}) of fixed dipoles and for a model of the L-type calcium channel with mobile structural charges inside the pore (*OX*). (b) The cross section of the channel is surrounded by active (white filled circles) dipoles. Note that *OX* is the only configuration in which channel charges are mobile whereas dipole charges are kept fixed for the entire simulation.

Section 2.3 describes the Induced Charge Computation (ICC) method. Finally, section 2.4 presents the treatment of boundary conditions for ion concentrations through a Grand Canonical Monte Carlo (GCMC) algorithm.

Some of these features have already been separately included in the simulation of electrolytes or ion channel permeation. In our work, these features have been consistently integrated to obtain an efficient and accurate particle-based numerical BD simulator for the realistic analysis of ion permeation through membrane pores.

Typycally, BD implementations use a "fixed charge" model to mimic ion channel charged groups: point charges (possibly obtained from PDB files) are embedded in the membrane and cannot move in response to ions' movement. This model can provide a satisfactory approximation in the case of wide pores (e.g., α-hemolysin and VDAC protein channels).[78,81,83]

However, a large number of ion channels (e.g., Ca^{2+} channels and K$^+$ channels) have a very narrow selectivity filter. In this case, permeating ions interact strongly with the protein charges in terms of electrostatic forces and steric repulsions. The result is a correlated motion of selectivity filter charges and ions in a very dense environment. In such a case, the "fixed charge" model appears to be inadequate. To provide a better description of ion motion in narrow pores, accounting for selectivity filter structural changes, we adopted a "mobile charge" model in which protein charges are treated similarly to other ions (i.e., they move according to BD) but are confined in the central section of the pore. This model is much more

challenging than the "fixed charge" model, requiring the evaluation of ion dynamics in crowded environments and the accurate evaluation of dielectric forces at each time step. We tackle these issues by introducing a novel retracing technique to safely handle unphysical ion configurations (which occur very frequently in the case of charge crowding) and by, for the first time, computing the dielectric forces on the fly. The use of these advanced techniques, and previously established techniques such as van Gunsteren and Berendsen integration and GCMC, allows us to study narrow and crowded channels, extending the applicability of BD, limited, until now, to wide ion channels.[42,43,77,78,80,81,89−91] The source code of our BROWNian Ion channel and Electrolyte Simulator (BROW-NIES) is available for free download at www.phys.rush.edu/BROWNIES.

2. OVERVIEW OF THE SIMULATOR

In this section, we present the main characteristics of the simulator using a simple model of a selective ion channel as a test bed to illustrate the main concepts. Although our 3-D simulator can handle structures with complex geometries, in this paper, we limit the analysis to a pore featuring a rotational symmetry—a reasonable assumption for ion channels—in order to simplify the simulation domain, to ease the explanation of the methodologies.

The simulation domain consists of a rectangular box featuring, at its center, a planar membrane oriented on the x−y plane that separates two ionic baths representing the intra-

and extracellular environments. Ions can flow from one bath to the other through a pore set at the center of the septum. A 2-D schematic section of the simulated system is shown in Figure 1a. The 3-D simulation domain with the 3-D channel structure is obtained by rotating the 2-D section in Figure 1a around the pore (z) axis. Unless otherwise stated, in our simulations we use different dielectric constants for water ($\varepsilon_W = 80$) and the membrane ($\varepsilon_M = 10$).

With the "fixed charge" model, we use two rings of six dipoles embedded in the membrane (light gray region) at $z = \pm 3$ Å to model the selectivity filter of the channel. Dipole negative charges (empty circles, -1 e each) are set 2 Å far from the dielectric boundary, and the positive charges (filled circles, 1 e each) are 3 Å further inside the membrane (E_6 configuration in Figure 1b). The dipoles produce a potential well within the pore that attracts cations and repels anions, resulting in a cation-selective channel. Furthermore, we added two other rings of six dipoles at the mouths of the channel whose charges and orientation allows us to control the spatial extent of the potential well created by the filter dipoles, thus enhancing the selectivity of the channel; the configuration adopted in this work includes negative charges (-1 e each) located at $z = \pm 7$ Å and $r = 8$ Å and positive charges (1 e each) located at $z = \pm 8$ Å and $r = 11$ Å.

In this paper, we describe the capabilities of our BD implementation by means of simulation of various channel models that differ in the configuration of their active dipoles (Figure 1b). The N_0 configuration models an uncharged channel and has no dipoles (mouth and filter), while the E_6 configuration has all the dipoles (mouth and selectivity filter). In the C_{31}, C_{32}, and C_{33} configurations, only three out of six filter dipoles in each ring are present (all mouth dipoles remain active).

We also use the "mobile charge" model to simulate narrow and crowded pores simulating a model of a L-type calcium channel. We use 8 half-charged oxygens to mimic its carboxylate-rich selectivity filter (OX configuration in Figure 1b). Oxygen ions are not linked to a fixed position and are moved the same as other ions, except they are confined in the central region of the pore ($z = \pm 5$ Å) with a hard wall potential. In this case, no dipoles are present in the membrane. This setup has been successfully used to study conduction properties of the open calcium channels[66,92−101] and allows us to deal with a realistic model of a narrow ion channel in BD for the first time.

Ions are free to move according to BD in the whole simulation domain except for the membrane. Details on the computation of ion motion are provided in section 2.2.

Ion concentrations within the bulk solutions are controlled by adding two control cells to the simulation domain (dark gray regions in Figure 1a) on both sides of the membrane. The control cells are placed at the far sides of the simulation domain (from $z = -100$ Å to $z = -70$ Å and from $z = 70$ Å to $z = 100$ Å, respectively). In the control cells ions move according to BD and their average concentration is controlled by the periodic execution of a GCMC algorithm (details in section 2.4).

Figure 2 illustrates the execution flow of our BD tool. The simulation setup (top box) consists of the initialization of the simulation domain and of the ions' position. Then, the chemical potentials of the ionic species in the baths are evaluated by an iterative GCMC routine (GCMC module). The main loop of our Brownian simulator involves three main blocks: the periodic execution of a GCMC routine to maintain the
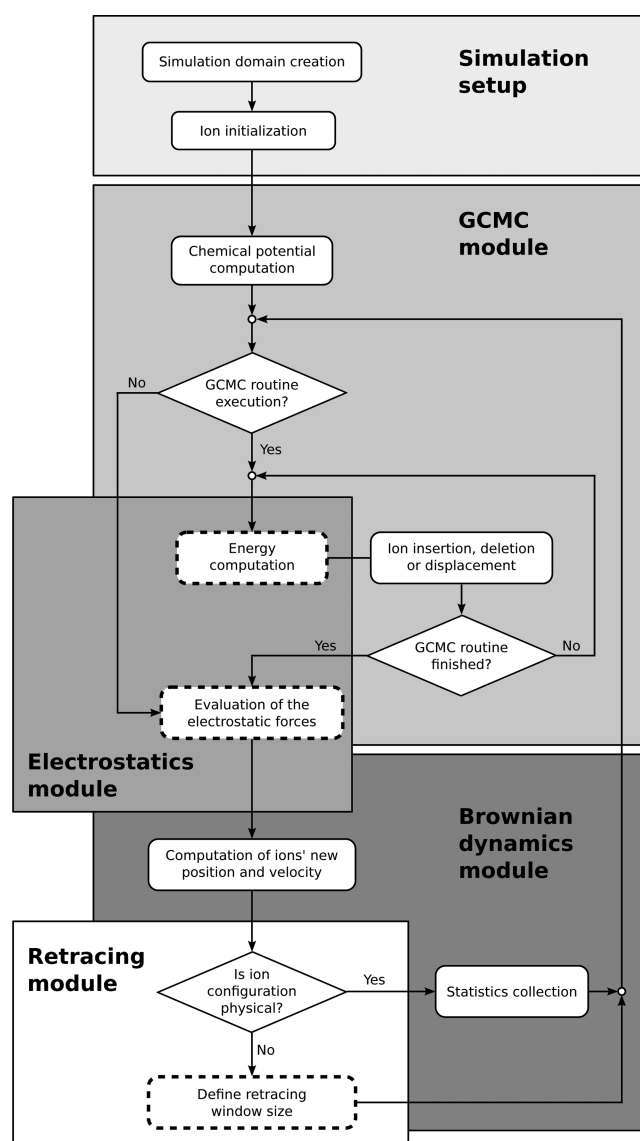
Figure 2. Simulation flow diagram. The five components of the simulator are highlighted by different backgrounds. The techniques introduced into BD by this paper (ICC dielectric force computation and the retracing technique) are highlighted with dash contours.

prescribed ion concentrations in the baths using the precalculated values for electrochemical potentials (GCMC module), the update of ions' positions and velocities as well as other statistics (BD module), and the evaluation of the electrostatic forces (for the BD module) and the electrostatic potentials (for the GCMC module) exerted on the ions with the ICC method (Electrostatic module). The retracing module, introduced in this paper, checks the ions' position and velocity. In the case of unphysical configurations, it takes care of retracing the simulation to a previous "safe" step (details in section 2.1).

We use periodic boundary conditions along the x-, y- and z-directions. When an ion flows out of the simulation box, it is reinserted on the opposite side of the simulation domain. When ion reinsertion is performed along z, ionic concentrations in baths are changed momentarily, but the GCMC routine preserves the prescribed concentrations on average.

The channel currents for each ionic species are evaluated at each BD time step using the Ramo−Shockley theorem:

$$I_\nu(t_n) = \frac{1}{1\text{Volt}} \sum_i^{N_\nu} q_i \mathbf{E}(\mathbf{r}_i, t_n) \mathbf{v}_i(t_n) \tag{1}$$

where q_i, $\mathbf{E}(\mathbf{r}_i)$, and ν_i are the charge, the electric field at ion's position $\mathbf{r}_i$ and the velocity of the i-th ion, respectively.[102–104] $\mathbf{E}(\mathbf{r}_i)$ is evaluated solving the Laplace Equation (i.e., removing all charges (ions and membrane charges) from the simulation domain) and applying a potential difference of 1 V (left to right ends). The sum runs over the N_ν ions of species ν.

Channel conductance is evaluated by averging the ionic current values sampled via the Ramo–Shockley theorem. This approach provides more robust statistics and faster convergence of the estimator with respect to the conventional approach, that is, counting ion channel-crossing events.[43,91,105] This is particularly helpful for channels of very low conductance for which the number of crossing events would be inadequate for reliable current estimation.

For each configuration, we simulate ion motion for at least 5 μs. This allows us to obtain reliable results on ion permeation without the need to average results of a number of simulations. An analysis of the variance of current estimation as a function of simulated time is provided in the Supporting Information.

The values for the ions' physical parameters are shown in Table 1: ionic radii are those defined by Pauling[1] and diffusion coefficients are set according to reference.[106]

Table 1. Ions' Physical Parameters Used in the Simulations

ion	valence	mass ($\times 10^{-27}$ kg)	radius (Å)	diff. coefficient ($\times 10^{-9}$ m²/s)
K$^+$	1	65.3967	1.33	1.96
Cl$^-$	−1	59.2995	1.81	2.03
Ca^{2+}	2	67.0353	0.99	0.79
Na$^+$	1	38.4532	0.95	1.33
O$^{1/2-}$	−0.5	26.552	1.40	2.2

It is generally thought that an ion's mobility inside ion channels will be significantly smaller than in bulk solution due to charge crowding.[81,89,107] Our BD tool can handle such a position-dependent diffusion coefficient in the channel. Results for a test case are in the Supporting Information.

2.1. Retracing Module. A critical issue affecting BD simulations of narrow pores is unphysically long ion jumps. This is particularly significant for the problem at hand because of charge crowding occurring inside the pore. During a time step, ions can get very close to each other, due to random forces. In such a case, the short-range repulsive electrostatic force evaluted at the next time step becomes so large that its application during the whole subsequent time step Δt leads to unphysically long ion jumps, possibly pushing ions out of the simulation domain or into the membrane. This error can be minimized by reducing Δt, leading to increased simulation time and reduction of the number of significant digits while evaluating finite difference derivatives. On the other hand, this error could be avoided by correctly taking into account the variation of the electrostatic and steric forces during each time step, as the distance between ions changes. In this case, the equations of motion become nonlinear and their solution requires iterative loops within the numerical integration procedure. The downside is, again, a larger computational burden.

These problems related to ion configurations are often overlooked in BD simulations, and a standard technique to treat such exceptions is not yet established. While a clear explanation of their treatment is not present in some implementations,[75,77,85,87,90] other BD implementations look for unphysical configurations caused by long jumps. When such configurations occur, the status of the ions is set back by one time step, the ions involved are identified, and their positions and velocities are arbitrarily changed in order to avoid the too-long ion flight.[43,91]

Here, we present a new procedure to rigorously treat unphysical ion configurations, without introducing artifacts caused by the change of ions' position or velocity. The basic idea is that, in case of an unphysical ion configuration, the simulation is retraced to a previous "safe" step, which may be several steps in the past. Then, the simulation restarts with the generation of a different sequence of random numbers.

Retracing the simulation by a single time step, as is done by other BD simulators, might not always avoid unphysical ion configurations (e.g., in case of ion crowding in the selectivity filter, see section 2.2.3). The result is an infinite loop in search of a physical configuration. For this reason, our procedure allows the retracing of a variable number of time steps. If an unphysical configuration occurs at time $t = t_n$, the simulation is traced back by one step and then restarted. If an exception occurs again at $t = t_n$ or $t = t_{n-1}$, the number of retraced steps is increased by one, and the simulation is restarted. If another exception occurs before reaching $t = t_{n+1}$, the number of retraced steps is increased by one, and the simulation is restarted. Once time $t = t_{n+1}$ is eventually reached, the retracing procedure is finished, the number of retracing steps is reset to one, and the simulation continues until another exception occurs.

2.2. Brownian Dynamics Module. *2.2.1. Langevin Equation of Motion.* In the framework of the primitive model for ions in aqueous solution, the evolution of the ions' positions and velocities in time can be modeled with the full Langevin equation of motion:[108–112]

$$m_i \dot{\mathbf{v}}_i(t) = -m_i \gamma_i(\mathbf{r}_i(t)) \mathbf{v}_i(t) + \mathbf{F}_i(\mathbf{r}_i(t)) + \mathbf{R}_i(t) \tag{2}$$

where $\mathbf{r}_i$, $\mathbf{v}_i$, m_i, and γ_i are the position, the velocity, the mass and the friction coefficient of particle i, respectively.[29,68] Equation 2 breaks up the force that acts on the i-th ion into three components: a random force ($\mathbf{R}_i(t)$), a frictional force ($-m_i \gamma_i(\mathbf{r}_i(t)) \mathbf{v}_i(t)$), and the systematic force ($\mathbf{F}_i(\mathbf{r}(t))$). The random and frictional forces represent the effects of ion collisions with the surrounding water molecules. The three directional components of the random force are uncorrelated and can be described by a stationary Markov process with Gaussian distribution, zero mean value, not correlated to other forces; on the other hand, the frictional force is proportional to the ion velocity. The magnitude of both depends on the friction coefficient $\gamma_i(\mathbf{r}_i(t))$, which is related to the diffusion coefficient $D_i(\mathbf{r}_i(t))$ through the Einstein relation:

$$D_i(\mathbf{r}_i(t)) = \frac{kT}{m_i \gamma_i(\mathbf{r}_i(t))} \tag{3}$$

where k and T are the Boltzmann constant and the temperature, respectively.[68,113–115] By defining a position-dependent diffusion coefficient we can account for different ion mobilities in the channel.

The systematic force is the sum of all the forces other than those caused by the surrounding water molecules. In our model, it is the sum of two contributions: a short-range

repulsive force that prevents ion overlap and the electrostatic forces from the sources of electric field in the system, such as electrical charges and transmembrane potential.

The short-range force that accounts for ions' finite size, preventing the overlap of the ions' electronic clouds, is modeled with the following inverse power formula:[43,85,116]

$$\mathbf{F}_{ij}^{SR} = \frac{|q_i q_j|}{4\pi\varepsilon_0\varepsilon|\mathbf{r}_i - \mathbf{r}_j|(p + 1)}\left(\frac{R_i + R_j}{|r_i - r_j|}\right)^p \hat{\mathbf{r}}_{ij} \quad (4)$$

where R_i, r_i, and q_i are the radius, the position and the charge of the i-th ion, respectively. ε is the permittivity of the medium where ions i and j are set, p is a hardness parameter that represents the strength of the interaction (we assume $p = 12$ following reference[75]), and $\hat{\mathbf{r}}_{ij}$ is the unit vector pointing from the i-th to the j-th ion centers. An analogous approach is adopted to model the repulsion of ion i from the membrane or channel wall ($R_j = 0$). The description of the numerical evaluation of the electrostatic force is described in section 2.3.

Some BD implementations assume that ion motion always occurs in the high friction limit. In this case, ion interaction with the surrounding water molecules is so strong that ions always move in a diffusive regime and the systematic force is by far dominated by the random force. The left-hand side of eq 2 (representing the inertial term) becomes negligible, resulting in the reduced Langevin equation:

$$\dot{\mathbf{r}}_i(t) = \frac{D_i(\mathbf{r}_i(t))}{kT}\mathbf{F}_i(\mathbf{r}_i(t)) + \hat{\mathbf{R}}_i(t) \quad (5)$$

where $\hat{\mathbf{R}}_i(t)$ is a random Gaussian variable with $\langle\hat{\mathbf{R}}_i\rangle = 0$ and $\langle\hat{\mathbf{R}}_i^2\rangle = 6D_i(\mathbf{r}_i(t))\Delta t$, where Δt is the time step used in the integration.

The approximation of damped motion of particles has been widely applied in numerous simulations of electrolytes and ion channels.[77,117] These simulators produce flux using this equation on the microscopic level even though Eisenberg et al. showed that this equation applied for averaged distributions does not produce a flux.[112] The discrepancy arises from the fact that, in the simulations, the reduced Langevin is applied to each ion at the microscopic level and not to the macroscopic ion ensemble. Flux is produced by adding an external driving force to the Hamiltonian of the system in terms of boundary conditions for the potential and/or the ion concentrations.

The assumption of the diffusive regime holds for bulk electrolytes, but there is no evidence for its accuracy in the presence of a membrane slab and, in particular, inside narrow pores. In confined spaces (e.g., in the selectivity filter of an ion channel), crowding becomes extremely important and plays a key role in ion motion. Therefore, in our opinion, it is vital to model ion dynamics according to eq 2.

2.2.2. Numerical Integration of the Langevin Equation. Many algorithms have been proposed to integrate eq 2 in order to evaluate the ions' motion.[29,68,74,118−122] We employed the method of van Gunsteren and Berendsen, since it proved to be highly reliable and accurate.[43,68,105,116]

At each time step t_n (of duration Δt), we evaluate for ion i the new position $\mathbf{r}_i(t_{n+1})$:

$$\begin{aligned}
\mathbf{r}_i(t_{n+1}) &= \mathbf{r}_i(t_n)(1 + e^{-\gamma_i\Delta t}) - \mathbf{r}_i(t_{n-1})e^{-\gamma_i\Delta t} \\
&+ \frac{\mathbf{F}_i(t_n)\Delta t}{m_i\gamma_i}(1 - e^{-\gamma_i\Delta t}) + \frac{\dot{\mathbf{F}}_i(t_n)\Delta t}{m_i\gamma_i^2}\left(\frac{\gamma_i\Delta t}{2}(1 + e^{-\gamma_i\Delta t})\right. \\
&\left. - (1 - e^{-\gamma_i\Delta t})\right) + \mathbf{X}_i^n(\Delta t) + e^{-\gamma_i\Delta t}\mathbf{X}_i^n(-\Delta t)
\end{aligned} \quad (6)$$

and its velocity:

$$\begin{aligned}
\mathbf{v}_i(t_n) = &\left[\mathbf{r}_i(t_{n+1}) - \mathbf{r}_i(t_{n-1}) + \frac{\mathbf{F}_i(t_n)}{m_i\gamma_i^2}G_i - \frac{\dot{\mathbf{F}}_i(t_n)}{m_i\gamma_i^3}G_i \right. \\
&\left. + \mathbf{X}_i^n(-\Delta t) - \mathbf{X}_i^n(\Delta t)\right]\frac{H_i}{\Delta t}
\end{aligned} \quad (7)$$

where $G_i = e^{\gamma_i\Delta t} - 2\gamma_i\Delta t - e^{-\gamma_i\Delta t}$, $H_i = \gamma_i\Delta t/(e^{\gamma_i\Delta t} - e^{-\gamma_i\Delta t})$ and $\mathbf{X}_i^n$ is a random variable defined as $\mathbf{X}_i^n = (1/m_i\gamma_i)\int_{t_n}^{t_n+\Delta t}(1 - e^{-\gamma_i(t_n+\Delta t-t)})\mathbf{R}_i(t)\,dt$. For a detailed description of $\mathbf{X}_i^n$, G_i, and H_i, the reader is referred to ref 68. In case of a position-dependent diffusion coefficient, $\gamma_i(t) = \gamma_i(\mathbf{r}_i(t))$ in eqs 6 and 7. For each ion i at location $\mathbf{r}_i(t_n)$, $\gamma_i(\mathbf{r}_i(t_n))$ is used throughout the time step. γ_i can change from time step to time step as ion i enters or exits the channel and moves to position $\mathbf{r}_i(t_{n+1})$, but it is assumed constant during a single time step in eqs 6 and 7. Therefore, we can use the same integration technique for both constant and varying γ_i.

This approach has two major advantages: high accuracy (higher order terms are included in the integration) and low sensitivity to time step duration (Δt is not subject to the condition $\Delta t \ll \gamma_i^{-1}$). Thanks to these features, this method allows us to treat ion motion both in bulk solution, where the frictional forces dominate, resulting in a diffusive regime, and near and within the channel, where ion motion is determined by short-range electrostatic and steric forces due to charge crowding.

2.2.3. Assessement and Validation. The accuracy of our Brownian engine was tested through several simulations for the simple case of bulk electrolytes. As documented in the Supporting Information, our implementation succeeds in describing ion motion correctly under different conditions in terms of solution composition, ion concentrations, and applied electric fields.

The relevance and the impact of unphysical ion configurations detected by long jumps exceptions (LJE) (discussed in section 2.1), is analyzed by comparing the results of the full Langevin equation (LAN) (eq 2) and the reduced Langevin equation in the high friction limit (HFL) (eq 5). Our results show that LAN is less sensitive to LJE at relatively large Δt values. The sensitivity of LAN and HFL models to LJE is estimated by the percentage of LJE events over the total number of steps (LJE%) and by the distribution of the number of back-trace steps needed to circumvent such events (N_{BT}).

First, we considered a rectangular box with periodic boundaries filled by various ionic solutions; no membrane or channel is present. Under different conditions for ion mixtures, electric fields applied to the solutions, and time step durations (1−100 fs), for both LAN and HFL, LJE% is limited to 0.1. The two methods produce identical results in terms of ion transport (velocity distributions, radial distribution functions) and solution properties (ion distribution, ion currents) (data not shown).
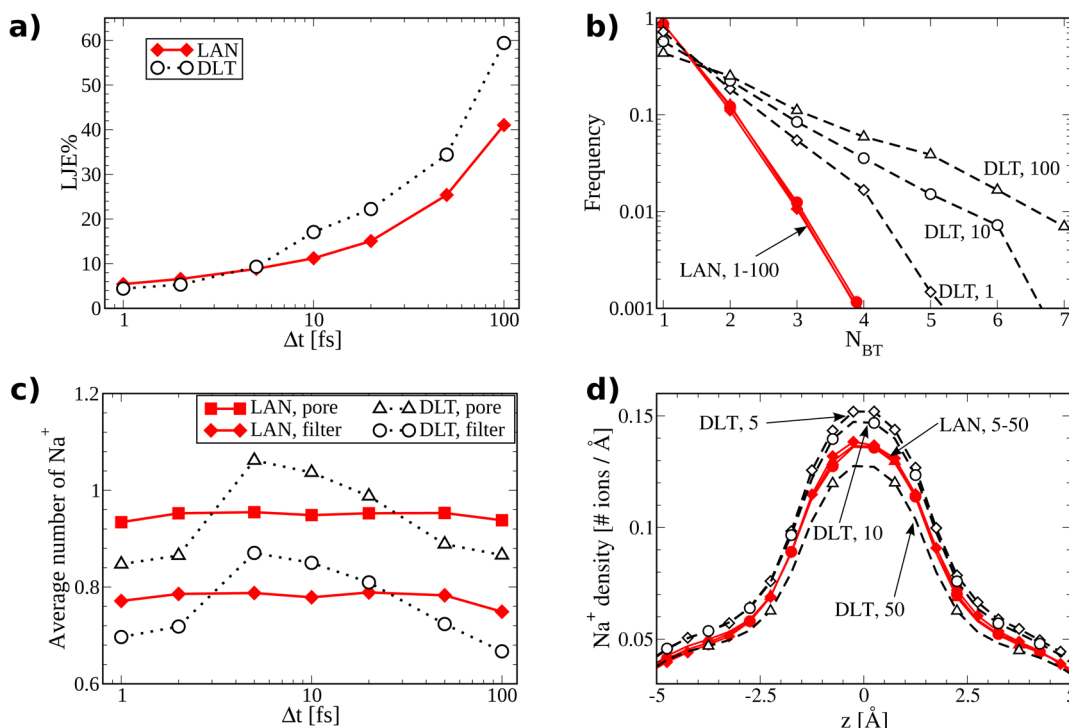
Figure 3. (Color online) Percentage of the number of long jump exception events over the total number of steps (LJE%) for full Langevin (LAN) and reduced Langevin in the high friction limit (HFL) motion integration for the simulation of a model calcium channel (*OX* configuration in Figure 1b). Left and right baths contained 100 mM NaCl and 0 mM NaCl (infinite dilute) solution, respectively. LAN describes ion motion more carefully requiring a smaller number of rejected steps (a). Retrace window size distribution (b) reveals that HFL needs larger retracing windows than LAN. Moreover, LAN is substantially insensitive to Δt (indicated by numbers, in fs) while HFL retrace window size increases with Δt. LAN is able to preserve the accuracy of ion motion description as Δt increases both in terms of channel occupancy (c) and ion distribution along the channel (d).

Then, we tested LAN and HFL using an uncharged channel (N_0 configuration in Figure 1b). We had a 100 mM NaCl solution in the left bath and a 0 mM NaCl (infinite dilute) solution in the right bath. Again, LAN and HFL provide essentially the same results (independent of time step duration in the 1−100 fs range) for ion distribution along the simulation domain (in particular inside the channel) and for ion currents. This is essentially due to very low average number of ions present in the channel (<0.1, data not shown).

Finally, we compared LAN and HFL in the case of the more complex *OX* configuration (see Figure 1b), where 8 oxygens model the selectivity filter of the L-type calcium channels.[92−94,98] The charge crowding occurring in the pore, due to the high density of oxygens in the central region of the pore, represents a numerical challenge for both LAN and HFL. In both cases the simulation overhead LJE% increases with the time step duration Δt and is limited to 10% for $\Delta t < 5$ fs (Figure 3a). For larger values of Δt, LAN performs significantly better than HFL.

Figure 3a also gives a qualitative picture of the numerical difficulties introduced by the "mobile charges" selectivity filter model. Unphysical ion configurations are very frequent in such dense systems, and their treatment with simpler techniques is detrimental and can easily affect the simulation results. In this view, our retracing technique is vital to obtain reasonable results in a reasonable amount of time.

The distribution of back-trace length, N_{BT}, provides important information about the capability of the Brownian simulation to circumvent forbidden configurations; the shorter the retracing window, the more efficient the algorithm is. In the LAN case, the retrace window length never exceeds 4

(necessary only once over 1000 LJE events) and is independent of Δt (Figure 3b). On the other hand, HFL needs a larger retrace window length that significantly increases with Δt.

Figure 3c shows the average number of Na$^+$ ions in the pore ($z = \pm 10$ Å) and in the selectivity filter ($z = \pm 5$ Å) obtained with LAN and HFL for different Δt. Figure 3d shows the Na$^+$ ion distribution along the pore obtained with LAN and HFL for different Δt. Both Figure 3c and d show how LAN preserves the accuracy of ion motion description as the time step duration increases.

These results show that, due to the missing inertial term (left-hand-side of eq 2), HFL is more prone to LJE and its accuracy is significantly degraded for increasing Δt. According to our analysis, the LAN description of ion motion with the van Gunsteren and Berendsen integration scheme and 5 fs $< \Delta t <$ 10 fs represents a good trade off between accuracy and simulation time.

2.3. Electrostatics Module: Evaluation of Fields and Systematic Forces. In order to determine ions' positions and velocities, via eq 2, it is necessary to compute the systematic force $\mathbf{F}_i(\mathbf{r}(t))$ acting on each ion in the system. As described in section 2.2, this force is the sum of short-range and long-range electrostatic contributions. The latter arises directly from the electric field generated by all the source charges located inside the simulation domain, from the charges that generate the applied field, and from the polarization charges induced by these on the dielectric interfaces. The accurate and fast evaluation of electrical forces is a crucial aspect for the simulation of charged particles in general and is particularly critical for the simulation of nanometer-scale structures. The

relation between electrical charges and electrostatic forces is described by the Poisson equation:

$$-\varepsilon_0 \nabla[\varepsilon(\mathbf{r})\nabla\Phi(\mathbf{r})] = -\rho(\mathbf{r}) \qquad (8)$$

where ε_0 is the permittivity of free space and $\rho(\mathbf{r})$ is the charge density of free charges. Free charges include the ionic, the electrode, and the structural protein charges. The ionic charges are point charges at the centers of ions, while the electrode charges are uniform surface charges $\pm\,\sigma$ at the boundaries of the system (at ± 100 Å in Figure 1a) producing an applied electric field $\mathbf{E}_Z^T$ along the z (normal to the membrane) direction that defines the transmembrane potential.[123,124]

The formulation of the electrostatic problem (primitive model for electrolytes; well-defined uniform dielectric regions separated by sharp rigid boundaries) lends itself to preserving the discreteness of charges, through the explicit evaluation of interparticle Coulombic forces and employing Boundary Element Methods (BEM) to treat the case of inhomogeneous dielectrics. In particular, BEMs exploit the Poisson equation to evaluate the polarization surface charges induced at the boundaries between different dielectric regions where a discontinuity of permittivity is located.[94,125−135]

Once the polarization surface charges are converted into equivalent point charges, the electric field can be evaluated everywhere in space as the superposition of Coulombic contributions from two sets of point charges: the source charges (e.g., the ions) and the charges induced at the dielectric boundaries.[94,128−131,133,135−141]

BEMs feature three major advantages with respect to classical finite differences/finite elements Poisson solver: (i) BEMs require only the discretization of the 2-D dielectric boundary instead of the discretization of the whole 3-D simulation domain; (ii) the ions' charges are not converted into equivalent charge densities, preserving the discrete nature of charged particles; and (iii) electrostatic forces are evaluated only at the ions' exact positions, and thus, no interpolation between values computed on a grid of points is needed.[94,132,133,135]

Note that, for homogeneous dielectric media, there are no polarization charges and the evaluation of the electrostatic forces is obtained applying Coulomb's law to source charges only. For this reason, some simple BD implementations assumed the same dielectric constant for water and membrane.[77] Although this approach considerably reduces the computational effort, it neglects reaction field effects, that are relevant in narrow pores (i.e., surface charges induced on the membrane and pore wall by ions).[141,142]

Some previous works accounted for polarization induced charges by using an iterative BEM.[42,43,91,143] Its huge computational burden made its run-time usage impractical. To circumvent this problem, the electrostatic forces were evaluated in advance on a grid of points for a large number of ion configurations and then stored in lookup tables. During the simulations, the forces exerted on the ions were evaluated as the superposition of elemental contributions obtained by interpolating between lookup table entries. This approach involves two kinds of limitations: (i) the loss in accuracy due to interpolation between table entries and (ii) only charge distributions featuring rotational symmetry can be simulated, since the number of grid points needed to solve the Poisson equation accurately in a fully asymmetrical 3-D system makes calculations and storage unfeasible.[42,43,80,91,105,143,144]

We tackle the electrostatic problem by employing the Induced Charge Computation (ICC) method, a BEM proposed by Boda et al.[94] In ref 132, we showed that for a given level of accuracy and for the same number of surface discretization elements, ICC is ∼2 orders of magnitude faster than iterative BEM[42,43,91,143] and is therefore much better suited for the simulation of membrane pores. The accuracy and speed of ICC allows run-time solution of the Poisson equation and, therefore, lookup tables are not required and asymmetric 3-D systems can be simulated as easily as symmetric ones.

The evaluation of induced charges with ICC is briefly discussed in section 2.3.1. For a more detailed description, please refer to refs 94, 130, 133, 134, and 137.

2.3.1. Evaluation of the Induced Surface Charges at the Dielectric Boundaries. For the problem at hand, the simulation domain is divided into two homogeneous regions by a sharp boundary $\mathcal{B}$: a low-permittivity region representative of the membrane layer and of the protein ($\varepsilon_M = 10$) and a high-permittivity region representative of the aqueous solution ($\varepsilon_W = 80$) (Figure 1a).

Mobile ions and fixed membrane/protein charges are treated as point charges. We can rewrite eq 8 in a form that emphasizes the relation between the polarization vector $\mathbf{P}(\mathbf{r})$ and the electric field $\mathbf{E}(\mathbf{r})$:

$$\varepsilon_0 \nabla\mathbf{E}(\mathbf{r}) = \rho(\mathbf{r}) - \nabla\mathbf{P}(\mathbf{r}) \qquad (9)$$

where $\mathbf{P}(\mathbf{r}) = (\varepsilon(\mathbf{r}) - 1)\varepsilon_0\mathbf{E}(\mathbf{r})$ accounts for the permittivity discontinuity. Polarization effects can be modeled via the polarization charge density $h(\mathbf{r}) = -\nabla\mathbf{P}(\mathbf{r})$ that is induced at $\mathcal{B}$ only, because the surface of each source charge is neglected.

Starting from eq 9, after some mathematical manipulations it is possible to express $h(\mathbf{s})$:[94,130,133]

$$h(\mathbf{s}) + \frac{\Delta\varepsilon}{4\pi\overline{\varepsilon}}\mathbf{n}(\mathbf{s})\int_{\mathcal{B}} \frac{\mathbf{s} - \mathbf{s}'}{|\mathbf{s} - \mathbf{s}'|^3}h(\mathbf{s}')\mathrm{d}\mathbf{s}'$$

$$= -\frac{\Delta\varepsilon}{4\pi\overline{\varepsilon}}\mathbf{n}(\mathbf{s})\left[\sum_k \frac{q_k}{\varepsilon(\mathbf{r}_k)}\frac{\mathbf{s} - \mathbf{r}_k}{|\mathbf{s} - \mathbf{r}_k|^3} + \frac{\mathbf{E}_z^T}{\varepsilon_W}\right] \qquad (10)$$

where $\Delta\varepsilon$ and $\overline{\varepsilon}$ are the difference and the arithmetic mean value, respectively, of the dielectric coefficients across the $\mathcal{B}$ surface, $\mathbf{n}(\mathbf{s})$ is the unit vector normal to $\mathcal{B}$ at $\mathbf{s}$, and $\varepsilon(\mathbf{r}_k)$ is the dielectric constant at charge q_k position $\mathbf{r}_k$. In eq 10, the integral is performed over the entire boundary surface $\mathcal{B}$. The right-hand side includes the contributions to the polarization charge by all the point source charges (ions or membrane/protein charges) and by the applied electric field, $\mathbf{E}_Z^T$, producing the transmembrane potential (applied voltage).

$\mathbf{E}_Z^T$ is the solution of the Laplace equation (i.e., Poisson equation with source charges removed) with prescribed electrical potentials on the system's boundaries (Dirichlet boundary conditions) and removing the dielectrics. For a simple simulation box such as ours, the solution is a constant electric field, producing an applied potential changing linearly between 0 and the value of the voltage (see the red dotted line in Figure 4a). $\mathbf{E}_Z^T$ also represents a source term in eq 10; thus, it induces charges on the dielectric boundaries that, in turn, contribute to the electric field acting on ions (see the red dotted line in Figure 4b). Because of this, we do not need to include the dielectrics in the Laplace equation. If the cell is large enough, the charges induced by $\mathbf{E}_Z^T$ do not affect the potential at the system's boundaries (red dotted line in Figure 4c).

The prescribed voltage is also maintained if the effect of the ions is taken into account. The average electrical potential produced by the ions (green dashed line in panel c has two
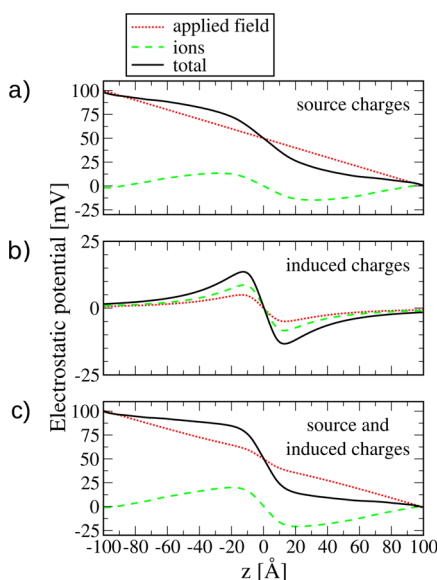
Figure 4. (Color online) Time-averaged electrical potentials along the channel axis from a simulation for the uncharged N_0 configuration. The baths contained 100 mM NaCl. The applied electric field, $\mathbf{E}_z^T = 5 \times 10^6$ V/m, produced a transmembrane potential of 100 mV. (a) Potential from source (free) charges: ionic charges (green dashed line) and electrode charges (red dotted line). (b) Potential from polarization charges induced by either the ions or the applied field (same line types as in part a). (c) Sum of the source and induced terms (same line types as in part a).

components: the average potential produced by the ions directly and the average potential of their polarization charges induced on $\mathcal{B}$ (green dashed lines in panels a and b, respectively). As seen in Figure 4, the average effects of both terms vanish at the system's boundaries. This means that the prescribed voltage is imposed at the system's boundaries on average. Of course, a fully self-consistent treatment of electrostatics would require the solution of the Poisson equation with the imposed Dirichlet boundary conditions "on the fly" as pointed out by Crozier et al.[145] and Hollerbach and Eisenberg.[146] In this case, the electrode charges would fluctuate and the potential of the ions would be zero at the boundaries not only on average but at every instant of the simulation. The solution used in this work, however, provides a good approximation. The approximation becomes better with increasing system size because the ions in the channel would have less influence on the fluctuating electrode charge. This approach has been used to perform MD simulations of electrolytes separated by an impermeable membrane[123,124,147,148] and in previous BD simulations of ion channels.[43,91,105,149]

We evaluate the integral in eq 10 by discretizing the dielectric boundary into S surface elements, named tiles, and approximating the induced charge density h_i over a single tile of area a_i as a point charge $h_i a_i$ located at its centroid $\mathbf{s}_i$. This produces a matrix formulation of eq 10 in the form

$$\mathbf{Ah} = \mathbf{b} \qquad (11)$$

where $\mathbf{A}$ is a $S \times S$ matrix describing the interactions between the S tiles, $\mathbf{b}$ is the electric field normal to each surface element
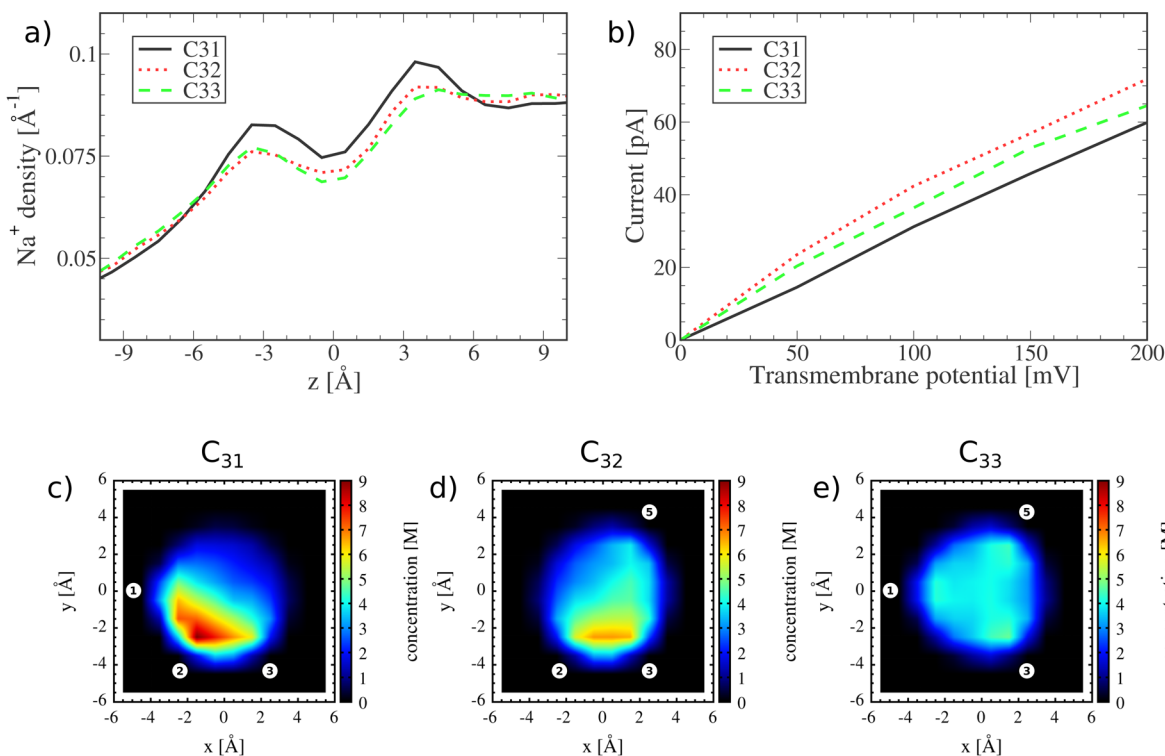
Figure 5. (Color online) Asymmetrically charged channel. C_{31}, C_{32}, and C_{33} configurations provide very similar Na$^+$ distributions along the pore (a) but different Na$^+$ currents (b) due to the different cross-sectional arrangement (c), (d) and (e). Na$^+$ ions pack in correspondence of the active dipoles (white-filled numbered circles). Note that Cl$^-$ ions are excluded from the pore due to the unfavorable dipole orientation. Na$^+$ distributions along the pore were obtained by dividing the simulation domain in slices along z, counting the average number of ions per slice and dividing by the slice thickness.

due to any source of electric field in the system (ions, membrane/protein charges, and transmembrane potential), and the vector $\mathbf{h}$ contains the polarization charges induced on the surface elements.[94,130,133] Within the ICC formulation, the elements of the matrix $\mathbf{A}$ are defined as

$$A_{ij} = \delta_{ij} + \frac{\Delta\varepsilon(s_i)}{4\pi\bar{\varepsilon}(s_i)} \int_{\mathcal{B}_j} \frac{(s_i - s')n(s_i)}{|s_i - s'|^3} ds' \quad (12)$$

and each element of vector $\mathbf{b}$ is

$$b_i = -\frac{\Delta\varepsilon(\mathbf{s}_i)}{4\pi\bar{\varepsilon}(\mathbf{s}_i)}\mathbf{n}(s_i)\left[\sum_k \frac{q_k}{\varepsilon(\mathbf{r}_k)} \frac{\mathbf{s}_i - \mathbf{r}_k}{|\mathbf{s}_i - \mathbf{r}_k|^3} + \frac{\mathbf{E}_z^T}{\varepsilon_W} \right] \quad (13)$$

where $\mathbf{s}_i$ is the centroid of the i-th boundary element and δ_{ij} is the Kronecker delta function. The integral in eq 12 is extended over the entire surface of the j-th tile. We approximate this integral by subdividing each tile into M subtiles as described in ref 94.

Solving eq 11 for $\mathbf{h}$, the induced surface charges are known and can be converted into point charges $(h_1a_1,h_2a_2,..,h_Sa_S)$ set at the tiles' centroids $(\mathbf{s}_1,\mathbf{s}_2,..,\mathbf{s}_{S})$. Then, the electric field acting on the i-th ion can be evaluated at its position $\mathbf{r}_i$ as a superposition of Coulombic contributions.

ICC's effectiveness lies in its matrix formulation: since the matrix $\mathbf{A}$ does not change throughout a simulation run (because the dielectric boundaries do not change shape and position), it can be inverted just once at the beginning of the simulation. Then, each electric force evaluation reduces to a matrix-vector product. This operation is relatively light computationally and allows for the solution of the Poisson equation at each time step. Moreover, the subtiling of every tile takes the curvature of the dielectric boundary into account properly, a feature absent in earlier BEM implementations,[126,130,137,150−153] with a relatively small number of tiles that still gives very accurate results.[94,130,133]

In each electrostatic calculation (Coulombic, ICC, and GCMC) we considered, in the x and y directions, the primary cell and two replicas of the primary cell (one left and one right), with the closest image replica convention. Instead, in the z direction we considered the system as an isolated box.

2.3.2. Assessment Analysis: The Case of Asymmetric Protein−Charge Spatial Distribution. The suitability of ICC for ion channel simulation, its accuracy and computational efficiency have been discussed extensively by the authors in refs 94, 132, 133, and 137. Here, we extend the assessment of this powerful method further by demostrating its applicability to asymmetrically charged ion channels.

We investigate current and selectivity in asymmetrically charged channels by switching off three out of the six filter dipoles in each ring (configurations C_{31}, C_{32}, and C_{33} of Figure 1b). In this study, all the mouth dipoles are switched on as in E_6 configuration. We performed simulations for each configuration and for different transmembrane potentials. The intra- and extracellular baths contained 100 mM NaCl solutions.

Figure 5a shows the Na$^+$ concentrations along the pore for the three configurations for a transmembrane potential of 100 mV. The different configurations produce very similar cross-section-averaged concentration profiles (almost identical for C_{32} and C_{33} configurations) with two small peaks near the filter dipole rings ($z = \pm 3$ Å). Similar results were obtained for different transmembrane potentials (data not shown).

Figure 5b shows Na$^+$ currents as functions of the transmembrane potential. At low transmenbrane voltage, all the configurations produce currents roughly proportional to the transmembrane potential, but feature distinctly different conductances. The most conductive configuration is C_{32}, while C_{31} is the least conductive one.

The analysis of cross-sectional Na$^+$ concentration maps at the right-most binding site allows us to analyze the link between the Na$^+$ permeation properties and the distribution of protein charges (Figure 5c, d, and e, for C_{31}, C_{32}, and C_{33} configurations, respectively). Na$^+$ ions are attracted by the negative terminal of the dipoles (displayed by white-filled numbered circles), resulting in very different concentration patterns. Although the total concentration is roughly the same for the three configurations (the average number of Na$^+$ ions occupying the pore is 1.55, 1.52, and 1.51 for C_{31}, C_{32}, and C_{33} respectively), the C_{31} configuration features a strong binding site due to three consecutive active dipoles, while C_{33} shows the most uniform-spreaded concentration because the active and inactive dipoles alternate. C_{32} is an intermediate case.

According to our results, strong ion localization within the selectivity filter due to the asymmetry of protein's charges leads to degradation of the channel conductance. The explanation of this effect is that the mobility of ions is reduced at the sites where ions accumulate. They are bound more strongly to the binding site by electrostatic attraction, so they are more reluctant to proceed through the channel. The effect of this competition between binding and conductance on selectivity was discussed in ref 98.

2.4. Interaction with the Surrounding Solution Bath: The Grand Canonical Monte Carlo Module. Mixtures of electrolytes, with different ionic species at very different concentrations, are common in biological systems (10^{-1} M K$^+$, 10^{-7} M Ca^{2+}, 10^{-3} M Mg^{2+} in the cytoplasm).[1,39,67] Indeed, almost all solutions inside cells are highly concentrated (more than 200 mM) with monovalent salts (i.e., namely more than 1−50 mM, according to the standards of physical chemistry) but contain less than 10^{-6} M Ca^{2+}. Ideally, the simulation of membrane pores should model the actual physiological conditions or experimental setup. However, due to limited computational resources, only a limited portion of the intra- and extracellular regions can be included in the simulation domain, making the treatment of ion and energy exchange with the surrounding solution baths challenging.

Early BD works employed a small simulation box where the number of ions was kept constant.[43,50,91] This approach does not provide a satisfactory representation of the whole baths and a rigorous treatment of boundary conditions since the simulated system was treated as isolated.[154,155] More recent implementations adopted two control cells, representative of the intra- and extracellular electrolytic baths, where the number of ions is kept constant in the control cells during the whole simulation run, while the total number of ions in the system could fluctuate.[42,156] This technique does not correctly model the energy exchange between the simulated system and the baths. Moreover, due to discreteness of ion charge, it is suitable only when concentrations and control cell dimensions allow one to deal with several ions for each ionic species, making submillimolar concentrations practically unmanageable.

Other works[42,77,81,90] used a Grand Canonical Monte Carlo (GCMC) algorithm, iteratively executed during the simulation, to force the prescribed time-averaged ionic concentrations and instantaneous chemical potential for each ionic species in the
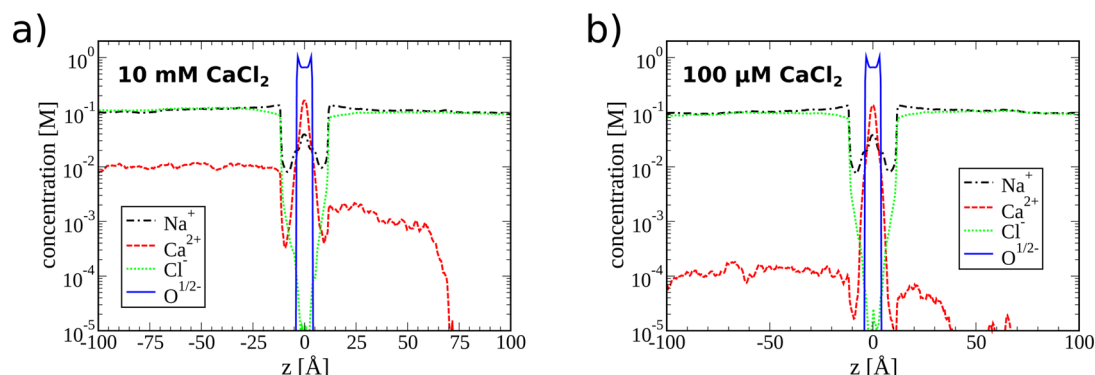
Figure 6. (Color online) Ion density profiles throughout the simulation domain for 10 mM (a) and 100 μM (b) CaCl$_2$ added to 100 mM NaCl on the left bath only. The right bath contains 100 mM NaCl. Concentrations were evaluated by dividing the simulation domain in slices along z, counting the average number of ions per slice and dividing by the volume of the slice. Our GCMC routine is able to ensure the prescribed concentrations in the baths.

control cells. This approach is based on the Dual Control Volume method of Heffelfinger and van Swol,[157] and it was applied to ionic systems by Im et al. for the first time.[77]

The GCMC approach is by far the most accurate and affordable for our purposes. Therefore, we maintain boundary conditions for ion concentrations in the control cells by employing a GCMC algorithm.[158] This setup has already been adopted successfully for the investigation of diffusion in chemical physics[159−163] and for the permeation of ion through ion channels.[65,77,81,90,98,164]

The GCMC algorithm allows concentration fluctuations but enforces constant time-averaged concentrations by performing individual ion insertions and deletions.[29,165,166] The insertion (deletion) probability p_ν^i (p_ν^o) of an ion of species ν is evaluated according to

$$p_\nu^{i/o} = \min\left\{1, \frac{N_\nu!}{(N_\nu + \chi)!} V^\chi \exp\left(\frac{-\Delta U + \chi\overline{\mu}_\nu}{kT}\right)\right\} \qquad (14)$$

where ΔU is the energy change associated with the insertion (deletion); k and T are the Boltzmann constant and the absolute temperature, respectively; N_ν is the number of ions of species ν in the control cell before the insertion (deletion); $\overline{\mu}_\nu$ is the chemical potential of the ion ν (that can be different in the two control cells); V is the control cell volume; and χ is 1 for the insertion and −1 for the deletion.

ΔU is the potential energy change of the particular ion distribution before and after the ion insertion (deletion); thus, it takes into account the energy of the whole system. On the other hand, $\chi\overline{\mu}_\nu$ is a global property of ion species ν that describes the energy needed to insert (remove) a ν ion in an electrolytic solution made up by different ionic species at given concentrations.

In the same way, the GCMC algorithm attempts ion displacements within the control cell with probability:

$$p_\nu^d = \min\left\{1, \exp\left(\frac{-\Delta U}{kT}\right)\right\} \qquad (15)$$

This method provides enough flexibility to deal with ionic concentrations from the molar down to the submillimolar range. At very low concentrations, however, sampling can be inadequate because of the very low probability of having ions in the control cells. This affects both the calculation of conductances and the ability of GCMC algorithm to ensure the prescribed ionic concentrations quickly. Treatment of

concentrations in the micromolar range (relevant in biological situations such as the L-type calcium channel[97,167]) requires special techniques to circumvent these problems that we do not consider here.[62,65] We pay attention to using wide control cells at large distances from the membrane to avoid altering ion distributions and dynamics in the vicinity of the channel and to provide ion screening from outside the simulation domain.

In our setup, preliminary iterative GCMC simulations provide accurate estimates of the chemical potentials inside the two control cells (dark gray regions in Figure 1a). The chemical potentials are computed for each ionic species, accounting for solution composition and temperature, with bulk GCMC simulations in a cubic simulation cell by means of an iterative method developed by Malasics and Boda[168,169] called the Adaptive GCMC (A-GCMC) method.

During the simulation, a GCMC cycle is periodically executed to preserve the correct ionic concentrations in the control cells. Each cycle performs ion insertion, deletion and displacement attempts, using eqs 14 and 15, with the chemical potential values calculated by the A-GCMC routine.

2.4.1. Assessment Analysis: Millimolar and Submillimolar Ion Concentrations. We investigated the ability of our GCMC routine to ensure boundary conditions for ion concentrations using the *OX* model (Figure 1b). Both baths contained 100 mM NaCl solutions. In addition, we added different concentrations of CaCl$_2$ solution to the left bath only. No transmembrane potential was applied.

Figure 6 shows ion density profiles throughout the simulation domain for 10 mM (a) and 100 μM (b) CaCl$_2$ added to 100 mM NaCl in the left bath only. In both cases, our GCMC is able to ensure the prescribed concentrations in the baths. Analogous results have been obtained for different ionic concentrations (data not shown).

In both cases, we executed a GCMC cycle every 10 ps (1000 BD steps with a time step of 10 fs). Each GCMC cycle consisted of 400 creation, 400 deletion (with eq 14), and 200 displacement (with eq 15) attempts for each ionic species in each individual control cell.

GCMC parameters (e.g., the number of creation, deletion and displacement attempts of each GCMC cycle, number of BD steps between two GCMC cycles) have a strong influence both on simulation accuracy and performance. For example, increasing the number of ion creation/deletion attempts in each GCMC routine helps to maintain the desired bulk concentrations. On the other hand, it requires a larger

computational effort. Optimal parameters are those that, for a given simulation, provide the desired boundary conditions with the minor computational effort.

GCMC parameters are strongly affected by the intrinsic properties of the simulated system (e.g., channel conductance, ion concentrations). Therefore, optimal parameters must be tailored for the specific system, and it is not possible to find GCMC parameter values with general validity, just as it is not possible to know how many time steps are needed to have a converged current. Without a rigorous mathematical analysis, which is beyond the scope of this paper, GCMC parameter optimization is a guess (parameter values) and check (ion concentrations) process.

3. CONCLUSION

A fully 3-D Brownian dynamics simulator of ion transport through membrane pores was presented. Although our tool can be adopted to investigate ion permeation through both synthetic nanopores and wide biological ion channels (e.g., α-hemolysin, VDAC),[78,81,83] it is specifically designed to treat with high accuracy the ion transport through narrow and crowded ion channels (e.g., Ca^{2+} and K^+ channels), where dielectric and steric effects are crucial issues. These kinds of channels have generally not been treated before with BD. Electrostatics in crowded pores, as well as crowding itself, are challenging issues that require the use of all the novel techniques introduced in our tool:

1. Unphysical ion configurations are handled rigorously with a novel retracing procedure; in case of such configurations, the simulation is retraced and restarted with the generation of new, different sequences of random numbers.
2. The dielectric calculation is tackled with the ICC method developed by Boda et al.[94] This accurate and efficient approach allows us to avoid the use of lookup tables and paves the way to fully 3-D simulations in asymmetric channels. This is the first time dielectric forces have been calculated on the fly in BD, to our knowledge.

Accuracy is also increased with the use of already well established techniques:

1. The common assumption of ion transport in the high friction limit is avoided in our approach; ion motion is evaluated by integrating the full Langevin equation with the discretization scheme of van Gunsteren and Berendsen,[68] allowing accurate calculation of ion motion, both in bulk solution and within narrow and crowded ion channels.
2. Boundary conditions for ion concentrations in the ionic baths are enforced with an accurate GCMC algorithm applied to two charge reservoirs. The use of the dual volume control-grand canonical algorithm[77,157] allows us to model submillimolar ion concentrations.

The key features and capabilities of the simulator have been extensively tested through the detailed analysis of several test cases. Accuracy, precision, and flexibility have been the guidelines for the implementation of all the software modules. All these aspects make our simulator a state-of-the-art tool for the study of ion permeation through membrane pores.

The source code of our tool, called BROWNIES (BROWNian Ion channel and Electrolyte Simulator), is available for free download at www.phys.rush.edu/BROWNIES (note that address is case sensitive).

ASSOCIATED CONTENT

Supporting Information

Results of assessment of Brownian dynamics implementation, comparison with Dynamic Monte Carlo, ionic currents variance, position-dependent diffusion coefficient and computational efficiency (Figures S1−S7). This material is available free of charge via the Internet at http://pubs.acs.org.

AUTHOR INFORMATION

Corresponding Author
*Email: Claudio_Berti@rush.edu.

Notes
The authors declare no competing financial interest.

ACKNOWLEDGMENTS

REFERENCES

(1) Hille, B. *Ionic Channels of Excitable Membranes*; Sinauer Associates: Sunderland, MA, 1992.
(2) Aidley, D.; Stanfield, P. *Ion Channels: Molecules in Action*; Cambridge University Press: Cambridge, U.K., 1996.
(3) Kew, J.; Davies, C. *Ion Channels: From Structure to Function*; Oxford University Press: New York, 2010.
(4) Fermini, B.; Priest, B. *Ion Channels*; Topics in Medicinal Chemistry; Springer: New York, 2008.
(5) Eisenberg, B. Ions in fluctuating channels: Transistors alive. *Fluct. Noise Lett.* **2012**, *11*, 1240001.
(6) Ashcroft, F. M. *Ion Channels and Disease*; Academic Press: San Diego, 2000.
(7) Maue, R. *Molecular Insights into Ion Channel Biology in Health and Disease*; Advances in Molecular and Cell Biology; Elsevier: Waltham, MA, 2004; Vol 32.
(8) Rouleau, G.; Gaspar, C. *Ion Channel Diseases*; Advances in Genetics; Elsevier Science, 2008.
(9) Bayley, H.; Cremer, P. S. Stochastic sensors inspired by biology. *Nat. Biotechnol.* **2001**, *413*, 226.
(10) Howorka, S.; Cheley, S.; Bayley, H. Sequence-specific detection of individual DNA strands using engineered nanopores. *Nat. Biotechnol.* **2001**, *19*, 636.
(11) Trojanowicz, M. Miniaturized biochemical sensing devices based on planar bilayer lipid membranes. *Fresenius' J. Anal. Chem.* **2001**, *371*, 246−260.
(12) Goryll, M.; Wilk, S.; Laws, G.; Thornton, T.; Goodnick, S.; Saraniti, M.; Tang, J.; Eisenberg, R. Silicon-based ion channel sensor. *Superlattices Microstruct.* **2003**, *34*, 451−457.
(13) Sugawara, M.; Kojima, K.; Sazawa, H.; Umezawa, Y. Ion-channel sensors. *Anal. Chem.* **1987**, *50*, 2842−2846.
(14) Bühlmann, P.; Aoki, H.; Xiao, K.; Amemiya, S.; Tohda, K.; Umezawa, Y. Chemical sensing with chemically modified electrodes that mimic gating at biomembranes incorporating ion-channel receptors. *Electroanalysis* **1998**, *10*, 1149−1158.
(15) Zugle, R.; Kambo-Dorsa, J.; Gadzekpo, V. Detection of metal ions using ion-channel sensor based on self-assembled monolayer of thioctic acid. *Talanta* **2003**, *61*, 837−848.
(16) Derrington, I.; Butler, T.; Pavlenok, M.; Collins, M.; Niederweis, M.; Gundlach, J. Nanopore sequencing with MspA. *Biophys. J.* **2009**, *96*, 316a.
(17) Dekker, C. Solid-state nanopores. *Nat. Nanotechnol.* **2007**, *2*, 209−215.

(18) Healy, K. Nanopore-based single-molecule DNA analysis. *Nanomedicine* **2007**, *2*, 459−481.

(19) Steinle, E.; Mitchell, D.; Wirtz, M.; Lee, S.; Young, V.; Martin, C. Ion channel mimetic micropore and nanotube membrane sensors. *Anal. Chem.* **2002**, *74*, 2416−2422.

(20) Branton, D.; et al. The potential and challenges of nanopore sequencing. *Nat. Nanotechnol.* **2008**, *26*, 1146.

(21) Iqbal, S. M.; Akin, D.; Bashir, R. Solid-state nanopore channels with DNA selectivity. *Nat. Nanotechnol.* **2007**, *2*, 243.

(22) Wanunu, M.; Sutin, J.; McNally, B.; Chow, A.; Meller, A. DNA translocation governed by interactions with solid-state nanopores. *Biophys. J.* **2008**, *95*, 4716−4725.

(23) Yusko, E. C.; Johnson, J. M.; Majd, S.; Prangkio, P.; Rollings, R. C.; Li, J.; Yang, J.; Mayer, M. Controlling protein translocation through nanopores with bio-inspired fluid walls. *Nat. Nanotechnol.* **2011**, *6*, 253.

(24) Hornblower, B.; Coombs, A.; Whitaker, R.; Kolomeisky, A.; Picone, S.; Meller, A.; Akeson, M. Single-molecule analysis of DNA-protein complexes using nanopores. *Nat. Methods* **2007**, *4*, 315−317.

(25) Zwolak, M.; Di Ventra, M. Colloquium: Physical approaches to DNA sequencing and detection. *Rev. Mod. Phys.* **2008**, *80*, 141−165.

(26) Tai, K.; Fowler, P.; Mokrab, Y.; Stansfeld, P.; Sansom, M. S. Molecular modeling and simulation studies of ion channel structures, dynamics and mechanisms. In *Methods in Nano Cell Biology*; Jena, B. P., Ed.; Academic Press: New York, 2008; Ch 12, Vol. *90*, pp 233−265.

(27) Kuyucak, S.; Andersen, O. S.; Chung, S.-H. Models of permeation in ion channels. *Rep. Prog. Phys.* **2001**, *64*, 1427.

(28) Tieleman, D. P.; C. Biggin, P.; R. Smith, G.; S. P. Sansom, M. Simulation approaches to ion channel structure−function relationships. *Q. Rev. Biophys.* **2001**, *34*, 473−561.

(29) Allen, P.; Tildesley, D. *Computer Simulation of Liquids*; Oxford Science Publications; Oxford University Press: New York, 1989.

(30) Jakobsson, E. Computer simulation studies of biological membranes: Progress, promise, and pitfalls. *Trends Biochem. Sci.* **1997**, *22*, 339−344.

(31) Roux, B. Theoretical and computational models of ion channels. *Curr. Opin. Struct. Biol.* **2002**, *12*, 182−189.

(32) Furini, S.; Domene, C. K⁺ and Na⁺ conduction in selective and nonselective ion channels via molecular dynamics simulations. *Biophys. J.* **2013**, *105*, 1737−1745.

(33) Fowler, P. W.; Abad, E.; Beckstein, O.; Sansom, M. S. P. Energetics of multi-ion conduction pathways in potassium ion channels. *J. Chem. Theory Comput.* **2013**, *9*, 5176−5189.

(34) Bernèche, S.; Roux, B. Energetics of ion conduction through the K⁺ channel. *Nature* **2001**, *414*, 73−77.

(35) Corry, B.; Thomas, M. Mechanism of ion permeation and selectivity in a voltage gated sodium channel. *J. Am. Chem. Soc.* **2012**, *134*, 1840−1846.

(36) Furini, S.; Domene, C. Gating at the selectivity filter of ion channels that conduct Na⁺ and K⁺ ions. *Biophys. J.* **2011**, *101*, 1623−1631.

(37) Boiteux, C.; Vorobyov, I.; Allen, T. W. Ion conduction and conformational flexibility of a bacterial voltage-gated sodium channel. *Proc. Natl. Acad. Sci. U.S.A.* **2014**, *111*, 3454−3459.

(38) Jensen, M. Ø.; Jogini, V.; Eastwood, M. P.; Shaw, D. E. Atomic-level simulation of current−voltage relationships in single-file ion channels. *J. Gen. Physiol.* **2013**, *141*, 619−632.

(39) Eisenberg, B. Multiple scales in the simulation of ion channels and proteins. *J. Phys. Chem. C* **2010**, *114*, 20719−20733.

(40) Bek, S.; Jakobsson, E. Brownian dynamics study of a multiply-occupied cation channel: Application to understanding permeation in potassium channels. *Biophys. J.* **1994**, *66*, 1028−1038.

(41) Mashl, R.; Tang, Y.; Schnitzer, J.; Jakobsson, E. Hierarchical approach to predicting permeation in ion channels. *Biophys. J.* **2001**, *81*, 2473−2483.

(42) Corry, B.; Hoyles, M.; Allen, T. W.; Walker, M.; Kuyucak, S.; Chung, S.-H. Reservoir boundaries in Brownian dynamics simulations of ion channels. *Biophys. J.* **2002**, *82*, 1975−1984.

(43) Chung, S.-H.; Allen, T. W.; Hoyles, M.; Kuyucak, S. Permeation of ions across the potassium channel: Brownian dynamics studies. *Biophys. J.* **1999**, *77*, 2517−2533.

(44) Allen, T.; Hoyles, M.; Kuyucak, S.; Chung, S. Molecular and Brownian dynamics study of ion selectivity and conductivity in the potassium channel. *Chem. Phys. Lett.* **1999**, *313*, 358−365.

(45) Eisenberg, B. Ionic channels in biological membranes—Electrostatic analysis of a natural nanotube. *Contemp. Phys.* **1998**, *39*, 447−466.

(46) Schuss, Z.; Nadler, B.; Eisenberg, R. S. Derivation of Poisson and Nernst−Planck equations in a bath and channel from a molecular model. *Phys. Rev. E* **2001**, *64*, 036116.

(47) Nonner, W.; Chen, D. P.; Eisenberg, B. Anomalous mole fraction effect, electrostatics, and binding in ionic channels. *Biophys. J.* **1998**, *74*, 2327−2334.

(48) Moy, G.; Corry, B.; Kuyucak, S.; Chung, S.-H. Tests of continuum theories as models of ion channels. I. Poisson−Boltzmann theory versus Brownian dynamics. *Biophys. J.* **2000**, *78*, 2349−2363.

(49) Corry, B.; Kuyucak, S.; Chung, S.-H. Tests of continuum theories as models of ion channels. II. Poisson−Nernst−Planck theory versus Brownian dynamics. *Biophys. J.* **2000**, *78*, 236−2381.

(50) Edwards, S.; Corry, B.; Kuyucak, S.; Chung, S.-H. Continuum electrostatics fails to describe ion permeation in the gramicidin channel. *Biophys. J.* **2002**, *83*, 1348−1360.

(51) Levitt, D. G. Modeling of ion channels. *J. Gen. Physiol.* **1999**, *113*, 789−794.

(52) Chen, D.; Jerome, J.; Eisenberg, R.; Barcilon, V. Qualitative properties of steady-state Poisson−Nernst−Planck systems: Perturbation and simulation study. *SIAM J. Appl. Math.* **1997**, *57*, 631−648.

(53) Radak, B.; Hwang, H.; Schatz, G. C. Modeling ion channels using Poisson−Nernst−Planck theory as an integrated approach to introducing nanotechnology concepts: The PNP cyclic peptide ion channel model. *J. Chem. Educ.* **2008**, *85*, 744.

(54) Zheng, Q.; Wei, G.-W. Poisson−Boltzmann−Nernst−Planck model. *J. Chem. Phys.* **2011**, *134*, 194101.

(55) Miedema, H.; Vrouenraets, M.; Wierenga, J.; Gillespie, D.; Eisenberg, B.; Meijberg, W.; Nonner, W. Ca²⁺ selectivity of a chemically modified OmpF with reduced pore volume. *Biophys. J.* **2006**, *91*, 4392−4400.

(56) Furini, S.; Zerbetto, F.; Cavalcanti, S. Role of the intracellular cavity in potassium channel conductivity. *J. Phys. Chem. B* **2007**, *111*, 13993−14000.

(57) Furini, S.; Domene, C.; Rossi, M.; Tartagni, M.; Cavalcanti, S. Model-based prediction of the α-hemolysin structure in the hexameric state. *Biophys. J.* **2008**, *95*, 2265−2274.

(58) Corry, B.; Kuyucak, S.; Chung, S. Invalidity of continuum theories of electrolytes in nanopores. *Chem. Phys. Lett.* **2000**, *320*, 35−41.

(59) Schmidt, M.; Brader, J. M. Power functional theory for Brownian dynamics. *J. Chem. Phys.* **2013**, *138*, 214101.

(60) Gillespie, D.; Nonner, W.; Eisenberg, R. S. Coupling Poisson−Nernst−Planck and density functional theory to calculate ion flux. *J. Phys.: Condens. Matter* **2002**, *14*, 12129.

(61) Marconi, U. M. B.; Tarazona, P. Dynamic density functional theory of fluids. *J. Chem. Phys.* **1999**, *110*, 8032−8044.

(62) Boda, D.; Gillespie, D. Steady state electrodiffusion from the Nernst−Planck equation coupled to local equilibrium Monte Carlo simulations. *J. Chem. Theory Comput.* **2012**, *8*, 824−829.

(63) Eisenberg, B.; Hyon, Y.; Liu, C. Energy variational analysis of ions in water and channels: Field theory for primitive models of complex ionic fluids. *J. Chem. Phys.* **2010**, *133*, 104104.

(64) Horng, T.-L.; Lin, T.-C.; Liu, C.; Eisenberg, B. PNP equations with steric effects: A model of ion flow through channels. *J. Phys. Chem. B* **2012**, *116*, 11422−11441.

(65) Ható, Z.; Boda, D.; Kristóf, T. Simulation of steady-state diffusion: Driving force ensured by dual control volumes or local equilibrium Monte Carlo. *J. Chem. Phys.* **2012**, *137*, 054109.

(66) Boda, D.; Kovács, R.; Gillespie, D.; Kristóf, T. Selective transport through a model calcium channel studied by local

equilibrium Monte Carlo simulations coupled to the Nernst−Planck equation. *J. Mol. Liq.* **2014**, *189*, 100−112.

(67) Fawcett, W. *Liquids, Solutions, and Interfaces: From Classical Macroscopic Descriptions to Modern Microscopic Details*; Topics in Analytical Chemistry Series; Oxford University Press: New York, 2004.

(68) van Gunsteren, W.; Berendsen, H. Algorithms for brownian dynamics. *Mol. Phys.* **1982**, *45*, 637−647.

(69) Jardat, M.; Bernard, O.; Turq, P.; Kneller, G. R. Transport coefficients of electrolyte solutions from smart Brownian dynamics simulations. *J. Chem. Phys.* **1999**, *110*, 7993−7999.

(70) Turq, P.; Lantelme, F.; Friedman, H. L. Brownian dynamics: Its application to ionic solutions. *J. Chem. Phys.* **1977**, *66*, 3039−3044.

(71) Shi, H.-B.; Gao, G.-H.; Yu, Y.-X. Self-diffusion coefficients of ions in primitive model electrolyte solutions by smart Brownian dynamics simulation. *Fluid Phase Equilib.* **2005**, *228−229*, 535−540.

(72) Kröger, M. Simple models for complex nonequilibrium fluids. *Phys. Rep.* **2004**, *390*, 453−551.

(73) Dufreche, J.-F.; Bernard, O.; Turq, P. Transport in electrolyte solutions: Are ions Brownian particles? *J. Mol. Liq.* **2005**, *118*, 189−194.

(74) Ermak, D. L. A computer simulation of charged particles in solution. I. Technique and equilibrium properties. *J. Chem. Phys.* **1975**, *62*, 4189−4196.

(75) Marreiro, D.; Saraniti, M.; Aboud, S. Brownian dynamics simulation of charge transport in ion channels. *J. Phys.: Condens. Matter* **2007**, *19*, 215203.

(76) Schirmer, T.; Phale, P. S. Brownian dynamics simulation of ion flow through porin channels. *J. Mol. Biol.* **1999**, *294*, 1159−1167.

(77) Im, W.; Seefeld, S.; Roux, B. A grand canonical Monte Carlo−Brownian dynamics algorithm for simulating ion channels. *Biophys. J.* **2000**, *79*, 788−801.

(78) Im, W.; Roux, B. Ion permeation and selectivity of OmpF porin: A theoretical study based on molecular dynamics, Brownian dynamics, and continuum electrodiffusion theory. *J. Mol. Biol.* **2002**, *322*, 851−869.

(79) Vora, T.; Corry, B.; Chung, S.-H. Brownian dynamics investigation into the conductance state of the MscS channel crystal structure. *Biochim. Biophys. Acta, Biomembr.* **2006**, *1758*, 730−737.

(80) Li, S. C.; Hoyles, M.; Kuyucak, S.; Chung, S.-H. Brownian dynamics study of ion transport in the vestibule of membrane channels. *Biophys. J.* **1998**, *74*, 37−47.

(81) Noskov, S. Y.; Im, W.; Roux, B. Ion permeation through the α-hemolysin channel: Theoretical studies based on Brownian dynamics and Poisson−Nernst−Plank electrodiffusion theory. *Biophys. J.* **2004**, *87*, 2299−2309.

(82) Allen, T.; Chung, S. Brownian dynamics study of an open-state KcsA potassium channel. *Biochim. Biophys. Acta, Biomembr.* **2001**, *1515*, 83−91.

(83) Lee, K. I.; Rui, H.; Pastor, R. W.; Im, W. Brownian dynamics simulations of ion transport through the VDAC. *Biophys. J.* **2011**, *100*, 611−619.

(84) Henn, F.; Dutour, J. A microscopic flow model based on Brownian dynamics for simulating ionic diffusion in a 2D-channel geometry. *J. Non-Cryst. Solids* **2005**, *351*, 1447−1454.

(85) Krishnamurthy, V.; Chung, S.-H. Adaptive Brownian dynamics Simulation for estimating potential mean force in ion channel permeation. *IEEE Trans. Nanobiosci.* **2006**, *5*, 126−138.

(86) Tindjong, R.; Eisenberg, R. S.; Kaufman, I.; Luchinsky, D. G.; McClintock, P. V. E. Brownian dynamics simulations of ionic current through an open channel. *AIP Conf. Proc.* **2005**, *780*, 563−566.

(87) Song, C.; Corry, B. Ion conduction in ligand-gated ion channels: Brownian dynamics studies of four recent crystal structures. *Biophys. J.* **2010**, *98*, 404−411.

(88) Chung, S.-H.; Allen, T. W.; Kuyucak, S. Conducting-state properties of the KcsA potassium channel from molecular and brownian dynamics simulations. *Biophys. J.* **2002**, *82*, 628−645.

(89) Comer, J.; Aksimentiev, A. Predicting the DNA sequence dependence of nanopore ion current using atomic-resolution brownian dynamics. *J. Phys. Chem. C* **2012**, *116*, 3376−3393.

(90) Im, W.; Roux, B. Brownian dynamics simulations of ions channels: A general treatment of electrostatic reaction fields for molecular pores of arbitrary geometry. *J. Chem. Phys.* **2001**, *115*, 4850−4861.

(91) Chung, S.-H.; Hoyles, M.; Allen, T.; Kuyucak, S. Study of ionic currents across a model membrane channel using Brownian dynamics. *Biophys. J.* **1998**, *75*, 793−809.

(92) Nonner, W.; Eisenberg, B. Ion permeation and glutamate residues linked by Poisson−Nernst−Planck theory in L-type calcium channels. *Biophys. J.* **1998**, *75*, 1287−1305.

(93) Nonner, W.; Catacuzzeno, L.; Eisenberg, B. Binding and selectivity in L-type calcium channels: A mean spherical approximation. *Biophys. J.* **2000**, *79*, 1976−1992.

(94) Boda, D.; Valiskó, M.; Eisenberg, R. S.; Nonner, W.; Henderson, D.; Gillespie, D. The effect of protein dielectric coefficient on the ionic selectivity of a calcium channel. *J. Chem. Phys.* **2006**, *125*, 034901.

(95) Boda, D.; Valiskó, M.; Eisenberg, B.; Nonner, W.; Henderson, D.; Gillespie, D. Combined effect of pore radius and protein dielectric coefficient on the selectivity of a calcium channel. *Phys. Rev. Lett.* **2007**, *98*, 168102.

(96) Gillespie, D.; Boda, D. The anomalous mole fraction effect in calcium channels: A measure of preferential selectivity. *Biophys. J.* **2008**, *95*, 2658−2672.

(97) Boda, D.; Valiskó, M.; Henderson, D.; Eisenberg, B.; Gillespie, D.; Nonner, W. Ion selectivity in L-type calcium channels by electrostatics and hard-core repulsion. *J. Gen. Physiol.* **2009**, *133*, 497−509.

(98) Rutkai, G.; Boda, D.; Kristóf, T. Relating binding affinity to dynamical selectivity from dynamic Monte Carlo simulations of a model calcium channel. *J. Phys. Chem. Lett.* **2010**, *1*, 2179−2184.

(99) Boda, D.; Henderson, D.; Gillespie, D. The role of solvation in the binding selectivity of the L-type calcium channel. *J. Chem. Phys.* **2013**, *139*, 055103.

(100) Gillespie, D.; Xu, L.; Wang, Y.; Meissner, G. (De)constructing the ryanodine receptor: Modeling ion permeation and selectivity of the calcium release channel. *J. Phys. Chem. B* **2005**, *109*, 15598−15610.

(101) Gillespie, D. Energetics of divalent selectivity in a calcium channel: The ryanodine receptor case study. *Biophys. J.* **2008**, *94*, 1169−1184.

(102) Yoder, P.; Gartner, K.; Krumbein, U.; Fichtner, W. Optimized terminal current calculation for Monte Carlo device simulation. *IEEE Trans. Comput.-aided Des. Integr. Circuits Syst.* **1997**, *16*, 1082−1087.

(103) Nonner, W.; Peyser, A.; Gillespie, D.; Eisenberg, B. Relating microscopic charge movement to macroscopic currents: The Ramo−Shockley theorem applied to ion channels. *Biophys. J.* **2004**, *87*, 3716−3722.

(104) Eisenberg, B.; Nonner, W. Shockley−Ramo theorem measures conformation changes of ion channels and proteins. *J. Comput. Electron.* **2007**, *6*, 363−365.

(105) Hoyles, M.; Kuyucak, S.; Chung, S.-H. Computer simulation of ion conductance in membrane channels. *Phys. Rev. E* **1998**, *58*, 3654−3661.

(106) Robinson, R.; Stokes, R. *Electrolyte Solutions*, 2nd Revised ed.; Dover Books on Chemistry; Dover Publications: Mineola, NY, 2002.

(107) Mamonov, A. B.; Kurnikova, M. G.; Coalson, R. D. Diffusion constant of K⁺ inside Gramicidin A: A comparative study of four computational methods. *Biophys. Chem.* **2006**, *124*, 268−278.

(108) Coffey, W.; Kalmykov, Y.; Waldron, J. *The Langevin Equation: With Applications to Stochastic Problems in Physics, Chemistry, and Electrical Engineering*; Series in contemporary chemical physics; World Scientific Publishing Company Incorporated: Singapore, 2004.

(109) Evans, D.; Morriss, G. *Statistical Mechanics of Nonequilibrium Liquids*; Theoretical chemistry; Cambridge University Press: Cambridge, U.K., 2008.

(110) Cooper, K.; Jakobsson, E.; Wolynes, P. The theory of ion transport through membrane channels. *Prog. Biophys. Mol. Biol.* **1985**, *46*, 51−96.

(111) Cooper, K. E.; Gates, P. Y.; Eisenberg, R. S. Surmounting barriers in ionic channels. *Q. Rev. Biophys.* **1988**, *21*, 331−364.

(112) Eisenberg, R. S.; Klosek, M. M.; Schuss, Z. Diffusion as a chemical reaction: Stochastic trajectories between fixed concentrations. *J. Chem. Phys.* **1995**, *102*, 1767−1780.

(113) Einstein, A. *Investigations on the Theory of Brownian Movement*; Dover Publications: New York, 1956.

(114) Kramers, H. Brownian motion in a field of force and the diffusion model of chemical reactions. *Physica* **1940**, *7*, 284−304.

(115) Schuss, Z. *Theory and Applications of Stochastic Differential Equations*; Wiley Series in Probability and Statistics—Applied Probability and Statistics Section; Wiley: New York, 1980.

(116) Aboud, S.; Marreiro, D.; Saraniti, M.; Eisenberg, R. A Poisson P^{3}M force field scheme for particle-based simulations of ionic liquids. *J. Comput. Electron.* **2004**, *3*, 117−133.

(117) Yamaguchi, T.; Akatsuka, T.; Koda, S. Brownian dynamics simulation of a model simple electrolyte in solvents of low dielectric constant. *J. Chem. Phys.* **2011**, *134*, 244506.

(118) Brańka, A. C.; Heyes, D. M. Algorithms for Brownian dynamics simulation. *Phys. Rev. E* **1998**, *58*, 2611−2615.

(119) Ansell, G. C.; Dickinson, E. Sediment formation by Brownian dynamics simulation: Effect of colloidal and hydrodynamic interactions on the sediment structure. *J. Chem. Phys.* **1986**, *85*, 4079−4086.

(120) Melrose, J. R.; Heyes, D. M. Rheology of weakly flocculated suspensions: Simulation of agglomerates under shear. *J. Colloid Interface Sci.* **1993**, *157*, 227−234.

(121) Honeycutt, R. L. Stochastic Runge−Kutta algorithms. I. White noise. *Phys. Rev. A* **1992**, *45*, 600−603.

(122) Chirico, G.; Langowski, J. Calculating hydrodynamic properties of DNA through a second-order Brownian dynamics algorithm. *Macromolecules* **1992**, *25*, 769−775.

(123) Roux, B. The membrane potential and its representation by a constant electric field in computer simulations. *Biophys. J.* **2008**, *95*, 4205−4216.

(124) Gumbart, J.; Khalili-Araghi, F.; Sotomayor, M.; Roux, B. Constant electric field simulations of the membrane potential illustrated with simple systems. *Biochim. Biophys. Acta, Biomembr.* **2012**, *1818*, 294−302.

(125) Rush, S.; Turner, A. H.; Cherin, A. H. Computer solution for time-invariant electric fields. *J. Appl. Phys.* **1966**, *37*, 2211−2217.

(126) Miertus, S.; Scrocco, E.; Tomasi, J. Electrostatic interaction of a solute with a continuum. A direct utilizaion of ab initio molecular potentials for the prevision of solvent effects. *J. Chem. Phys.* **1981**, *55*, 117−129.

(127) Shaw, P. B. Theory of the Poisson Green's function for discontinuous dielectric media with an application to protein biophysics. *Phys. Rev. A* **1985**, *32*, 2476−2487.

(128) Yoon, B. J.; Lenhoff, A. M. A boundary element method for molecular electrostatics with electrolyte effects. *J. Comput. Chem.* **1990**, *11*, 1080−1086.

(129) Juffer, A. J.; Botta, E. F. F.; van Keulen, B. A. M.; van der Ploeg, A.; Berendsen, H. J. C. The electric potential of a macromolecule in a solvent: A fundamental approach. *J. Comput. Phys.* **1991**, *97*, 144−171.

(130) Bardhan, J. P. Numerical solution of boundary-integral equations for molecular electrostatics. *J. Chem. Phys.* **2009**, *130*, 094102.

(131) Kuyucak, S.; Hoyles, M.; Chung, S.-H. Analytical solutions of Poisson's equation for realistic geometrical shapes of membrane ion channels. *Biophys. J.* **1998**, *74*, 22−36.

(132) Berti, C.; Gillespie, D.; Eisenberg, R.; Fiegna, C. Particle-based simulation of charge transport in discrete-charge nano-scale systems: The electrostatic problem. *Nanoscale Res. Lett.* **2012**, *7*, 135.

(133) Berti, C.; Gillespie, D.; Bardhan, J. P.; Eisenberg, R. S.; Fiegna, C. Comparison of three-dimensional Poisson solution methods for particle-based simulation and inhomogeneous dielectrics. *Phys. Rev. E* **2012**, *86*, 011912.

(134) Boda, D.; Gillespie, D.; Nonner, W.; Henderson, D.; Eisenberg, B. Computing induced charges in inhomogeneous dielectric media: Application in a Monte Carlo simulation of complex ionic systems. *Phys. Rev. E* **2004**, *69*, 046702.

(135) Boda, D.; Varga, T.; Henderson, D.; Busath, D. D.; Nonner, W.; Gillespie, D.; Eisenberg, B. Monte Carlo simulation study of a system with a dielectric boundary: Application to calcium channel selectivity. *Mol. Simul.* **2004**, *30*, 89−96.

(136) Tausch, J.; Wang, J.; White, J. K. Improved integral formulations for fast 3-D method-of-moments solvers. *IEEE Trans. Comput.-Aided Des. Integr. Circuits Syst.* **2001**, *20*, 1398−1405.

(137) Bardhan, J. P.; Eisenberg, R. S.; Gillespie, D. Discretization of the induced-charge boundary integral equation. *Phys. Rev. E* **2009**, *80*, 011906.

(138) Liang, J.; Subramaniam, S. Computation of molecular electrostatics with boundary element methods. *Biophys. J.* **1997**, *73*, 1830−1841.

(139) Zauhar, R. SMART: A solvent-accessible triangulated surface generator for molecular graphics and boundary element applications. *J. Comput.-Aided Mol. Des.* **1995**, *9*, 149−159.

(140) Altman, M. D.; Bardhan, J. P.; White, J. K.; Tidor, B. Accurate solution of multi-region continuum biomolecule electrostatic problems using the linearized Poisson−Boltzmann equation with curved boundary elements. *J. Comput. Chem.* **2009**, *30*, 132−153.

(141) Levitt, D. Electrostatic calculations for an ion channel. I. Energy and potential profiles and interactions between ions. *Biophys. J.* **1978**, *22*, 209−219.

(142) Nadler, B.; Hollerbach, U.; Eisenberg, R. S. Dielectric boundary force and its crucial role in gramicidin. *Phys. Rev. E* **2003**, *68*, 021905.

(143) Hoyles, M.; Kuyucak, S.; Chung, S. Energy barrier presented to ions by the vestibule of the biological membrane channel. *Biophys. J.* **1996**, *70*, 1628−1642.

(144) Hoyles, M.; Kuyucak, S.; Chung, S.-H. Solutions of Poisson's equation in channel-like geometries. *Comput. Phys. Commun.* **1998**, *115*, 45−68.

(145) Crozier, P. S.; Henderson, D.; Rowley, R. L.; Busath, D. D. Model channel ion currents in NaCl-extended simple point charge water solution with applied-field molecular dynamics. *Biophys. J.* **2001**, *81*, 3077−3089.

(146) Hollerbach, U.; Eisenberg, R. S. Concentration-dependent shielding of electrostatic potentials inside the gramicidin A channels. *Langmuir* **2002**, *18*, 3626−3631.

(147) Jensen, M.Ø.; Borhani, D. W.; Lindorff-Larsen, K.; Maragakis, P.; Jogini, V.; Eastwood, M. P.; Dror, R. O.; Shaw, D. E. Principles of conduction and hydrophobic gating in k^+ channels. *Proc. Natl. Acad. Sci. U.S.A.* **2010**, *107*, 5833−5838.

(148) Tieleman, D.; Leontiadou, H.; Mark, A.; Marrink, S.-J. Simulation of pore formation in lipid bilayers by mechanical stress and electric fields. *J. Am. Chem. Soc.* **2003**, *125*, 6382−6383.

(149) Chung, S.-H.; Allen, T. W.; Kuyucak, S. Modeling diverse range of potassium channels with Brownian dynamics. *Biophys. J.* **2002**, *83*, 263−277.

(150) Tomasi, J.; Persico, M. Molecular interactions in solution: An overview of methods based on continuous distributions of the solvent. *Chem. Rev.* **1994**, *94*, 2027−2094.

(151) Mennucci, B.; Cammi, R.; Tomasi, J. Excited states and solvatochromic shifts within a nonequilibrium solvation approach: A new formulation of the integral equation formalism method at the self-consistent field, configuration interaction, and multiconfiguration self-consistent field level. *J. Chem. Phys.* **1998**, *109*, 2798−2807.

(152) Cammi, R.; Tomasi, J. Analytical derivatives for molecular solutes. II. Hartree−Fock energy first and second derivatives with respect to nuclear coordinates. *J. Chem. Phys.* **1994**, *101*, 3888−3897.

(153) Green, M. E.; Lu, J. Simulation of water in a small pore: Effect of electric field and density. *J. Phys. Chem. B* **1997**, *101*, 6512−6524.

(154) Nadler, B.; Naeh, T.; Schuss, Z. The stationary arrival process of independent diffusers from a continuum to an absorbing boundary is Poissonian. *SIAM J. Appl. Math.* **2001**, *62*, 433−447.

(155) Nadler, B.; Naeh, T.; Schuss, Z. Connecting a discrete ionic simulation to a continuum. *SIAM J. Appl. Math.* **2003**, *63*, 850−873.

(156) Corry, B.; Allen, T. W.; Kuyucak, S.; Chung, S.-H. Mechanisms of permeation and selectivity in calcium channels. *Biophys. J.* **2001**, *80*, 195−214.

(157) Heffelfinger, G. S.; van Swol, F. Diffusion in Lennard-Jones fluids using dual control volume grand canonical molecular dynamics simulation (DCV-GCMD). *J. Chem. Phys.* **1994**, *100*, 7548−7552.

(158) Valleau, J. P.; Cohen, L. K. Primitive model electrolytes 1. Grand canonical Monte-Carlo computations. *J. Chem. Phys.* **1980**, *72*, 5935−5941.

(159) Heffelfinger, G.; Ford, D. Massively parallel dual control volume grand canonical molecular dynamics with LADERA I. Gradient driven diffusion in Lennard-Jones fluids. *Mol. Phys.* **1998**, *94*, 659−671.

(160) Thompson, A.; Ford, D.; Heffelfinger, G. Direct molecular simulation of gradient-driven diffusion. *J. Chem. Phys.* **1998**, *109*, 6406−6414.

(161) Pohl, P.; Heffelfinger, G. Massively parallel molecular dynamics simulation of gas permeation across porous silica membranes. *J. Membr. Sci.* **1999**, *155*, 1−7.

(162) Thompson, A.; Heffelfinger, G. Direct molecular simulation of gradient-driven diffusion of large molecules using constant pressure. *J. Chem. Phys.* **1999**, *110*, 10693−10705.

(163) Rutkai, G.; Kristóf, T. Dynamic Monte Carlo simulation in mixtures. *J. Chem. Phys.* **2010**, *132*, 124101.

(164) Csányi, E.; Boda, D.; Gillespie, D.; Kristóf, T. Current and selectivity in a model sodium channel under physiological conditions: Dynamic Monte Carlo simulations. *Biochim. Biophys. Acta, Biomembr.* **2012**, *1818*, 592−600.

(165) Frenkel, D.; Smit, B. *Understanding Molecular Simulation: From Algorithms to Applications*; Computational Science; Elsevier Science: Amsterdam, 2001.

(166) Sadus, R. *Molecular Simulation of Fluids: Theory, Algorithms, and Object-Orientation*; Elsevier: Amsterdam, 2002.

(167) Sather, W. A.; McCleskey, E. W. Permeation and selectivity in calcium channels. *Annu. Rev. Physiol.* **2003**, *65*, 133−159.

(168) Malasics, A.; Gillespie, D.; Boda, D. Simulating prescribed particle densities in the grand canonical ensemble using iterative algorithms. *J. Chem. Phys.* **2008**, *128*, 124102.

(169) Malasics, A.; Boda, D. An efficient iterative grand canonical Monte Carlo algorithm to determine individual ionic chemical potentials in electrolytes. *J. Chem. Phys.* **2010**, *132*, 244103.